Structural and Mutagenesis Studies of Soluble Methane Monooxygenase Reductase from *Methylococcus capsulatus* (Bath)

by
Lisa L. Chatwood
B.S. Biochemistry
Miami University, 2001

SUBMITTED TO THE DEPARTMENT OF CHEMISTRY IN PARTIAL FULFILLMENT OF THE REQUIREMENTS FOR THE DEGREE OF

MASTER OF SCIENCE IN BIOLOGICAL CHEMISTRY
AT THE
MASSACHUSETTS INSTITUTE OF TECHNOLOGY

August 2004 [2004]

Signature of Author: _____

Department of Chemistry
August 6, 2004

Certified by: _____

Stephen J. Lippard
Arthur Amos Noyes Professor of Chemistry
Thesis Supervisor

Accepted by: _____

Robert W. Field
Chairman, Departmental Committee on Graduate Studies

Structural and Mutagenesis Studies of Soluble Methane Monooxygenase Reductase from *Methylococcus capsulatus* (Bath)

by
Lisa L. Chatwood

Submitted to the Department of Chemistry
on August 6, 2004, in Partial
Fulfillment of the Requirements for the Degree of
Master of Science in Biological Chemistry

ABSTRACT

The solution structure for the 27 kDa flavin binding domain of soluble methane monooxygenase reductase from *Methylococcus capsulatus* (Bath) was solved by NMR spectroscopy. The structure consists of a two domains, an FAD binding domain with a six-stranded antiparallel β-barrel and one α-helix, and an NADH binding domain with a five-stranded parallel β-sheet surrounded by four α-helices. The FAD cofactor is bound at the interface between the two domains in a novel conformation. Near this FAD cofactor, a conserved C-terminal phenylalanine residue is proposed to act as a conformational gate for electron transfer. Kinetic studies on a series of mutants confirm that this phenylalanine controls electron transfer by regulating access of NADH substrate to the bound flavin cofactor.

Thesis supervisor: Stephen J. Lippard
Title: Arthur Amos Noyes Professor of Chemistry

For my parents and my grandmother, who taught me
to use my head and follow my heart.

ACKNOWLEDGEMENTS

I would first like to thank my advisor, Professor Stephen Lippard, for all his help and guidance. I am very appreciative of his support throughout my graduate career and in my decision to follow a new path.

I am indebted to Jens Müller, who patiently taught me the ropes of working in the lab and techniques of NMR spectroscopy for macromolecules. He contributed several of the beautiful protein figures in Chapter 1. John Gross was also infinitely helpful in designing, running and interpreting new NMR experiments, as well as answering my many questions. Many thanks go to Professor Gerhard Wagner for his useful suggestions and use of spectrometers, and to the students and postdocs in his lab for all their help.

Thank you to the members of the MMO subgroup, Jessica Blazyk, Dan Kopp, Edna Ambundo, Matt Sazinsky, Elisabeth Cadieux, Laurance Beauvais, Leslie Murray, Mike McCormick, Viviana Izzo and Joey Bautista. You have taught me much, and it has truly been a pleasure to work with all of you. I am grateful to the rest of the Lippard lab as well, for your friendship and always willing assistance.

Many thanks go to my parents for their love, guidance and counseling sessions, and to my grandmother for her unconditional love. Thank you to my brothers Phillip, Jonathan and Adam for believing in my abilities and keeping me grounded. I am blessed to have such a family.

Thank you to Elizabeth, for reminding me not to let "the man" get me down. Thank you also to my drinking buddies Kris, Lara and Ralph, and to fellow bio folks Will, Mohammed, Daniel, Jessica and Sasha for helping me keep my sanity.

And finally, thank you to Jim for being my shoulder to cry on, the outlet for my angry vents, a compassionate ear that understood my worries and doubts, my constant and unwavering support, and enough of a 'nerd' to spend many late-night, long-distance phone calls talking shop with me.

TABLE OF CONTENTS

LIST OF TABLES AND SCHEMES

LIST OF FIGURES

Chapter 1: NMR Structure of the Flavin Domain of Soluble Methane Monooxygenase Reductase from *Methylococcus capsulatus* (Bath)

Introduction

Methane monooxygenases (MMOs) are multi-component enzyme systems with the extraordinary capability to oxidize the most inert of hydrocarbons, converting methane to methanol (*1-4*). They are expressed in methanotrophic bacteria, which use methane as their only source of energy and carbon. Since methanotrophs can oxidize a variety of other hydrocarbons and have been applied for bioremediation, they are of great chemical, biological as well as commercial interest (5,6).

The soluble methane monooxygenase (sMMO) from *Methylococcus capsulatus* (Bath) consists of four components, a 251 kDa hydroxylase MMOH, a 15.9 kDa coupling protein MMOB, a 38.7 kDa reductase MMOR and a 12 kDa protein of as yet unidentified function, MMOD (*7-9*). A full understanding of the mode of action of the enzyme requires the knowledge of the three-dimensional structures of its proteins. Investigations of the sMMO components from *M. capsulatus* (Bath) and other methanotrophs thus far have supplied X-ray crystal structures of MMOH (*10-14*) and NMR solution structures of MMOB (15,16) and the MMOR ferredoxin domain, MMOR-Fd, comprising 98 amino acids (*17*) .

Because of the fairly large size of MMOR and the presence of a paramagnetic [2Fe-2S] cofactor, solving the NMR structure of the complete protein is challenging. We therefore decided to pursue this task with a three-step strategy. First, the structure of the reduced form of the smaller, paramagnetic MMOR-Fd was determined (*17*). In the present report we describe the solution structure of the reduced form of the second, 250 amino acid domain, MMOR-FAD. We chose to investigate the structure of the fully reduced protein because of its greater stability and the better comparability with the MMOR-Fd domain, which was

solved previously in the reduced state. The entire MMOR structure will then be solved based on these two individual building blocks. Crystal structures of similar proteins, including phthalate dioxygenase reductase (*18*) and benzoate-1,2-dioxygenase reductase (*19*) have already been solved, providing good comparisons for an NMR structure. Ultimately, knowledge of this reductase structure, together with the three-dimensional structure of MMOH, will enable us to interrogate long-range electron transfer reactions within and between soluble methane monooxygenase proteins.

Materials and Methods

Expression of MMOR-FAD. An expression system for MMOR-FAD, the flavin domain of methane monooxygenase reductase, capable of growing on M9 minimal medium with high yields was produced by transforming the plasmid pFAD21 into competent *Escherichia coli* BL21(DE3) cells. The plasmid was constructed by cutting the gene coding for MMOR-FAD out of pRED-FAD (20) and inserting it into the pET21(+) vector system (Novagen, Inc.), substituting a T7 promoter for the tac promoter present in pRED-FAD. The cells were grown in M9 minimal medium at 37 °C with constant shaking at 200 rpm. A concentration of 100 mg L^{-1} ampicillin was used for selection. When the OD_{600} value of the cell suspension reached 0.6 (or 0.4 for D_2O-based medium), expression was induced by adding IPTG to a final concentration of 0.1 mM. Cells were harvested after 12-15 hours, and the protein was purified as described previously (20). The concentration of MMOR-FAD was determined by using an extinction coefficient of $\varepsilon_{458} = 11{,}300\ M^{-1}\ cm^{-1}$ (20). Because no FAD was added to any of the media, all

of the cofactor incorporated into the protein had to be synthesized by the *E. coli* bacteria. As a consequence, the FAD moiety always showed the same isotopic labeling pattern as the corresponding protein.

^{15}N-Labeling of the protein was achieved by introducing 1 g L^{-1} of $^{15}NH_4Cl$ in the medium. For uniform ^{13}C-labeled protein, 2 g L^{-1} of ^{13}C glucose was used. Biosynthetic fractional ^{13}C labeling was performed with 10% ^{13}C glucose. Two samples of triple-labeled protein with different levels of deuteration were obtained by using $^{15}NH_4Cl$, ^{13}C glucose and 70% and 99.9% D_2O, respectively. Perdeuterated MMOR-FAD samples with terminally $^{13}C,^{1}H$ methyl-labeled Ile, Leu and Val residues were obtained by adding [3-^{13}C]-α-ketobutyrate and [3,3'-^{13}C]-α-ketoisovalerate to the medium, as described previously (21,22). In addition, 150 mg L^{-1} of natural abundance Phe, Tyr and Trp were added at the same time as the ILV-precursors to obtain ^{1}H labeling of aromatic side chains. Perdeuterated MMOR-FAD samples with protonated Tyr and Trp or Phe side chains were prepared by adding ^{15}N labeled Phe or ^{15}N labeled Tyr and unlabeled Trp to media containing $^{15}NH_4Cl$, 1,2,3,4,5,6,6-^{2}H-D-glucose and 99.9% D_2O. For selective ^{15}N amide labeling of Val, Phe, Tyr and Leu residues, the plasmid pRED-FAD was transformed into competent *E. coli* DL39 cells, which are auxotrophs for Asp, Ile, Leu, Phe, Tyr and Val. The resulting cells were grown in M9 minimal medium supplemented with 100 mg L^{-1} of each of the six amino acids, one of them with a ^{15}N-labeled amide group. Reverse selective labeling of Arg residues was achieved by growing BL21(DE3)/pRED-FAD cells in M9 minimal medium supplemented with 1 g L^{-1} of $^{15}NH_4Cl$ and 100 mg L^{-1} of natural abundance Arg. All isotopically labeled minimal media components and

amino acids, with the exception of the ILV precursors, were purchased from Cambridge Isotope Laboratories.

NMR Experiments. NMR experiments were performed with reduced 0.6 – 1.0 mM MMOR-FAD in 50 mM Na phosphate buffer, final pH of 6.7 after addition of $Na_2S_2O_4$, with 1 mM DTT, 0.1% NaN_3 and 2 mM Pefabloc (Roche Diagnostics GmbH, Germany). A final amount of 30 mM $Na_2S_2O_4$ and 3 equiv of NADH had to be added to keep the protein reduced. NMR tubes were filled under a nitrogen atmosphere and flame sealed.

Spectra were acquired at 750 MHz (Varian Unity Inova), 600 MHz (Bruker DRX) or 500 MHz (Bruker DRX equipped with a cryoprobe, or Varian Inova) at 25 °C unless stated otherwise. Backbone resonance assignments were obtained by using three-dimensional TROSY heteronuclear experiments (HNCA, HN(CO)CA, HN(CA)CB, HN(COCA)CB, HNCO, HN(CA)CO) and selective labeling techniques (*23*). Side chain assignments were obtained by using H(C-CO)NH-TOCSY, (H)C(CO)NH-TOCSY, ^{15}N TOCSY-HSQC, ^{15}N NOESY-HSQC, and ^{13}C NOESY-HSQC experiments (*23*). Stereospecific assignments of the methyl groups of 13 Leu and 10 Val residues were obtained with biosynthetic fractional ^{13}C labeling (*24*). Distance constraints were collected from ^{15}N NOESY-HSQC (100 ms mixing time at 25 °C and 60 ms mixing time at 35 °C), ^{13}C NOESY-HSQC (100 ms mixing time, fully ^{13}C-labeled protein), ^{13}C HMQC-NOESY (80 ms mixing time, ILV-methyl labeled protein with additionally ^{1}H-labeled (a) Tyr and Trp and (b) Phe residues), and homonuclear proton NOESY experiments (60 ms mixing time). Additional long-range distance constraints were gathered from ^{15}N labeled, deuterated protein with protonated (a) Tyr and Trp or (b) Phe (180 ms, 25 °C) by ^{15}N NOESY-HSQC. Spectra were processed with FELIX (Molecular

Simulations Inc., San Diego) or PROSA (*25*) and analyzed with XEASY (*26*) on Silicon Graphics work stations. The dihedral angle constraints for ϕ and ψ used in the calculations were obtained with the computer program TALOS (*27*).

Structure Calculations. NOESY crosspeaks were integrated by using the integration routine in the program DYANA (28). Interatomic upper-distance limits were calculated with the program CALIBA (29) based on NOESY crosspeak intensities for shorter mixing time experiments, or by collecting peak volumes into several bins and converting to distance by a factor of r^{-6} for experiments with long mixing times. Initial structure calculations were performed on Silicon Graphics workstations with the computer program DYANA (28) using simulated annealing by molecular dynamics in dihedral angle space. At all stages of the calculations, hydrogen bond constraints were introduced for residues determined to be in an α helix or a β strand. For each hydrogen bond two constraints were included into the calculations, $d_{NH\cdots O} = 1.8 - 2.4$ Å and $d_{N\cdots O} = 2.8 - 3.4$ Å. Methyl-methyl and methyl-aromatic constraints were added in later stage simulated annealing calculations performed in X-PLOR (30).

The FAD cofactor was incorporated into calculations by creating topology and parameter files in the program XPLO2D (*31*) from pdb coordinates of FAD in the crystal structure of the NADPH:ferredoxin reductase (FdR) from *Azotobacter vinelandii* (PDB code 1A8P) (*32*). Hydrogen atoms were added to FAD to result in the species $FADH_2$, which was optimized in InsightII (Accelrys, Inc.) prior to conversion in XPLO2D. The files were appended to earlier protein simulated annealing calculations for final structure calculation, and structures were viewed

and statistics calculated using VMD (33). Protein figures were created with the program MOLMOL (34).

Results

NMR Experiments. Backbone heavy atom and C^{β} resonances were assigned by using eight TROSY triple resonance experiments (HNCA/HN(CO)CA for 70% and 99% protein deuteration levels, HN(CA)CB/HN(COCA)CB and HNCO/HN(CA)CO) and ^{15}N selective labeling of valine, phenylalanine, tyrosine and leucine, and reverse labeling of arginine residues as described previously (23,35). Resonances of 37 residues with extremely slowly exchanging amide protons were not detected in the triple resonance spectra of MMOR-FAD at the 99% deuteration level but could be assigned with an additional HNCA/HN(CO)CA pair when using protein with approximately 70% deuteration. These slow-exchanging protons were primarily found in the FAD-binding domain, including amide protons for amino acids 14-17, 27-32, 50-52, 54, 63-65, 69, 71, 73-79, 83, 85-88, 91-92 and 101-103. Residue 191 was the only amino acid of this type in the NADH-binding domain. Secondary structure elements were identified based on ^{13}C chemical shift indices (36), dihedral angle constraints obtained from the program TALOS (27), and an analysis of NOE crosspeak patterns in the ^{15}N NOESY-HSQC and ^{13}C NOESY-HSQC spectra typical for α helices and β strands.

Significant improvement of peak resolution in the aliphatic region of the ^{13}C, ^{1}H spectra was observed for ILV-F and ILV-YW labeled proteins, as shown in Figure 1-1. This gain in resolution is obtained not only by limiting the total

number of ^{13}C labeled groups, but also by providing spectra in which these protonated methyl groups are embedded in an otherwise perdeuterated background. A total of 247 methyl-methyl and methyl-aromatic constraints were collected from these experiments, greatly improving previously unstructured hydrophobic regions with few constraints. Additional long mixing time experiments on perdeuterated, ^{15}N labeled protein with protonated Phe or Trp and Tyr side chains allowed assignment of aromatic protons and provided further long-range distance information. Several constraints between backbone amide protons and aromatic side chains to the N3 amide proton of the isoalloxazine moiety were also obtained to constrain the cofactor.

Solution Structure. For structure calculation, a total of 3653 constraints were used. Included are 1559 intra-residue constraints, 671 sequential, 239 medium-range and 434 long-range NOE constraints, along with 247 methyl-methyl and methyl-aromatic NOE constraints from the spectra using ILV-labeled protein, 172 hydrogen-bond constraints and 331 dihedral angle constraints. Of these constraints, 21 NOE, 90 dihedral and two hydrogen-bond restraints were used to constrain the FAD cofactor within the protein structure. The core region of the protein, residues 10-250, has an average backbone rmsd of 0.98 Å for the set of 10 lowest energy structures. Average backbone rmsd values for secondary structures within individual domains, residues 10 to 111 for the FAD binding domain and 113 to 245 for the NADH binding domain, were 0.89 and 0.84, respectively. Structural statistics are summarized in Table 1. All calculated structures for MMOR-FAD converged, with the lowest energy structures containing no distance constraint violations greater than 0.5 Å or dihedral angle constraint violations greater than 5 degrees.

The NMR structure in Figure 1-2 reveals that MMOR-FAD consists of two domains, one containing the FAD cofactor and the other binding NADH. This structural feature is characteristic of proteins in the flavoprotein electron transferase family such as MMOR, phthalate dioxygenase reductase (PDR) (*18*), benzoate 1,2-dioxygenase reductase (BenC) (*19*) or NADPH:ferredoxin reductase (*32*). Figure 1-3a shows the sequence homology of MMOR-FAD to the flavin and NAD(P)H binding domains of these proteins. The FAD-binding domain of MMOR-FAD folds into a cylindrical six-stranded antiparallel β sheet and contains one α helix covering one opening of the cylinder. Many of the residues with slow-exchanging amide protons mentioned above are located within this β sheet, suggesting a rather rigid structure. The unstructured residues 2-10 are part of the linker between the Fd and FAD binding domains in the full-length protein. Residues 11-23 comprise strands Fβ1a and Fβ1b, which are broken by a loop region of residues 17-19 and are the first strand of the β-barrel. A tight loop back to strand Fβ2 (26-33) forms the next part of the sheet and is followed by a long, unstructured loop of residues 34 to 49. A short strand Fβ3 (50-53), loop and Fβ4 (62-65) continue the cylinder sheet, followed by another, shorter unstructured loop of residues 66-75, parallel to the longer unstructured loop (34-49). Strand Fβ5 (76-80) leads into a loop of residues 81-88, followed by helix Fα1 (89-94) along one end of the β-barrel structure, which leads into Fβ6 (101-105), also part of the β sheet. Residues 106 to 120 form a coil linking the two domains. There is a cleft between strands Fβ4 and Fβ5, between which the isoalloxazine moiety and ribotyl chain of FAD binds. Direct evidence for flavin ring binding is seen in

NMR spectra as discussed further below, and ribotyl chain binding is expected based on sequence homology to other flavin-binding proteins.

The NADH binding domain contains alternating beta strands and alpha helices forming a five-stranded parallel β sheet with two α helices positioned on each side of the sheet, thus resulting in a classical nucleotide binding fold. Residues 121 to 126 make up the central strand Nβ1 of this domain, followed by helix Nα1 comprising residues 130-143. After this helix, residues 144-148 loop leading into strand Nβ2 (149-154), next to Nβ1, followed by a long loop of residues 155-163 into helix Nα2 (164-173), then a short loop to strand Nβ3 (178-181) at the edge of the parallel β sheet. Another long loop leads to helix Nα3 with residues 199 to 207, followed by a loop to residues 213-217 in strand Nβ4 packed on the opposite side of strand Nβ1. A short loop leads into the long helix Nα4, with residues 220-233, which winds around in a long loop to strand Nβ5 (237-244). This final β strand sits next to Nβ4, finishing the β sheet with a strand order of Nβ3-Nβ2-Nβ1-Nβ4-Nβ5. The C-terminal tail loops back into the protein and rests between helices Nα2 and Nα3 and the β sheet.

FAD Cofactor Interactions. To constrain the FAD cofactor, a total of 21 FAD-protein and FAD-FAD NOEs were used, as well as one hydrogen bond, as shown in Figure 1-4. Both the C7 and C8 methyl groups on the flavin ring were observable in ^{13}C NOESY-HSQC spectra, and both the adenine-N6 amine and isoalloxazine-N3 amide protons were evident in ^{15}N NOESY-HSQC spectra. The ^{15}N chemical shifts of 147 ppm for N3 on the isoalloxazine ring and 79 ppm for AN6 on the adenine ring agree well with previously reported values of 145-154 ppm, for reduced flavins bound to proteins (*37-39*), and of 82-83 ppm, for free

^{15}N-labeled adenine, respectively (*40*). We were unable to definitively assign additional peaks to the FAD cofactor, due to the resolution of collected spectra and peak crowding in expected regions for chemical shifts. Assignment for remaining nitrogen atoms in FAD, as well as for ribityl and ribotyl carbon and hydrogen atoms was ambiguous. The crosspeaks for FAD HN3 are given in Figure 1-5, along with corresponding backbone amide peaks for residues Ser65, Leu79, Arg81 and Leu246, showing the presence of several short contacts between the latter residues and the isoalloxazine group. The unusual upfield shift of the Leu246 amide proton suggests that it is stacking on top of the isoalloxazine ring. The amide peak for conserved Phe88 is shifted downfield to 12.04 ppm in the ^{1}H dimension, ~2 ppm from other amide peaks in the spectrum. Furthermore, the magnitude of the peak in ^{15}N labeled, perdeuterated protein exchanged into water is much smaller than average amide peaks, suggesting slow exchange. Together, these results provide evidence for a stable hydrogen bond involving the Phe88 amide proton. Since the ^{15}N NOESY-HSQC spectra did not reveal the identity of the corresponding hydrogen bond acceptor, and because in early structure calculations this amide proton was pointing towards the AMP phosphate of the FAD cofactor, two hydrogen bond constraints were added during later stages of the calculation.

FAD is located at the interface between the domains (Figure 1-6), and converges in all structures with an rmsd value of 0.77 Å. The isoalloxazine moiety binds at the cleft between Fβ4 and Fβ5 in the FAD domain, with the C7M and C8M methyl groups protruding towards the linker between the two domains. The ribotyl chain extends along the cleft in the N-terminal domain β

sheet, and the AMP phosphate group binds along the loop between Fβ5 and Fα1, its negative charge being compensated by an arginine side chain (Arg87). Amino acids Thr128 / Gly129 and the C-terminal tail residues Phe245 and the amide proton of Leu246 lie near the *re*-face of the flavin ring. Experimental proof for this alignment can be found for example in the shielding of the Leu246 amide proton by the ring current effect of the flavin ring, resulting in an anomalous upfield shift (Figure 1-5). The N6 amine group of adenine is located along the loops between Nβ2 and Nα2 (residues 156-160) and Nβ3 and Nα3 (residues 187-189), creating an extended conformation of FAD with adenine binding along the edge of the domain interface away from the chain linking the domains. Figure 1-7 shows the FAD cofactor binding site and summarizes interactions between FAD and the protein.

Discussion

MMOR-FAD Structure. MMOR has high sequence homology to other members of the flavoprotein electron transferase family. The FAD/NADH binding domain of MMOR is structurally homologous to several other members of this class of proteins, most notably benzoate-1,2 dioxygenase reductase from *Acinetobacter* sp. strain ADP1 (*19*). Since BenC has an identical arrangement of ferredoxin, FAD and NADH binding domains, MMOR can be expected to have a similar structure. The structures for the FAD and NADH binding domains in both proteins are similar, with an rmsd value of 3.8 Å for superimposed structures. The major difference between these proteins occurs at the C-

terminus, where the MMOR tail folds back into the NADH binding domain, whereas BenC has a tail extending to the surface of the protein.

The FAD binding domain in MMOR is composed of an antiparallel β barrel with an α helix at one opening of the barrel. This domain is structurally homologous to other FAD binding domains. Residues binding the FAD cofactor are strictly conserved within the reductase proteins of soluble MMO of methanotrophs, as shown in Figure 1-3b. The FAD itself is in an extended conformation so that the adenine moiety is distal from the isoalloxazine ring. This arrangement of the cofactor is unlike any conformation previously determined in the X-ray crystal structure analyses of homologous proteins (Figure 1-8d). Those structural studies resulted either in a bent conformation having the AMP moiety folding back towards the flavin ring or in an "extended" conformation where adenine is oriented away from it. In the bent conformation, the adenine group is held in place by hydrogen bonds involving its N6 and N7 nitrogen atoms and O3' of the ribityl moiety (FdR, Figure 1-8c; BenC, Figure 1-8a) (18,19,32) with or without additional stabilization by stacking of an aromatic residue in the C-terminal region of the protein (Phe255 in FdR, Trp248 in flavodoxin reductase (FlxR) (*41*), no stacking in BenC). In the previously established "extended" conformation, no hydrogen bonding within the cofactor was observed. Instead, stacking on a tyrosine side chain within an extended loop in the N-terminal domain preceding Fα1 was used for stabilization (Tyr120 in spinach ferredoxin-$NADP^+$ reductase (FNR), Figure 1-8b; Tyr104 in *Anabaena* FNR) (*42-44*). In the conformation found in MMOR-FAD, neither stacking on an aromatic side chain nor intra-residue hydrogen bonding is observed for the

adenine moiety. Because of the presence of only a short loop between Fβ6 and Fα1, this behavior was predicted previously (*41*). The negative charge of the FAD phosphate groups is compensated by arginine side chains Arg62 and Arg87 (Figure 1-6), the first of which is strictly conserved within the sMMO family (Figure 1-3), and a hydrogen bond from the Phe88 amide group at the N-terminus of Fα1. Similar charge neutralization occurs in several other proteins of the flavodoxin reductase family (32,41,43). The isoalloxazine ring is in a very similar environment in all of the structures mentioned above, including MMOR-FAD. Nearly all structures display stacking of an aromatic residue from the C-terminal region of the protein (Phe245 in MMOR-FAD, none in FdR, Phe335 in BenC, Tyr247 in FlxR, Tyr314 in spinach FNR, Tyr303 in *Anabaena* FNR) on the *re*-face of the flavin ring, and all of them feature a non-perpendicular stacking interaction with a conserved tyrosine from the N-terminal domain on the *si*-face (Tyr64 in MMOR–FAD, Tyr53 in FdR, Tyr158 in BenC, Tyr52 in FlxR, Tyr95 in spinach FNR, Tyr79 in *Anabaena* FNR). The conserved tyrosine interaction with the *si*-face of the flavin ring has been proposed to be responsible for the correct positioning of the cofactor (*45*).

The loops at the end of the β barrel opposite to Fα1, residues 34-49 and 65-75, are less structured than the rest of the domain. In the crystal structures of PDR and BenC (*19*), the ferredoxin domain, which is missing in MMOR-FAD, is located in this region of the protein, suggesting that the disorder found here might arise from the absence of the ferredoxin domain in MMOR-FAD. The full-length structure of MMOR should resolve or further explain this discrepancy as well as that of the unusual FAD conformation. Additionally, the unstructured N-

terminal chain should have a defined structure as a linker region between the ferredoxin and FAD binding domains.

NADH binding to MMOR-FAD could not be observed by NMR spectroscopy. No detectable signal of or crosspeaks to bound NADH, present in threefold excess in the solution, could be assigned in the NMR spectra. This result is not surprising considering in its reduced form the protein has no requirement to bind additional NADH. Based on sequence homology to other FNR proteins crystallized with NAD(P)H analogues, NADH is expected to bind at the carboxy-terminal edge of Nβ1 and Nβ4 of the parallel β sheet (19,43). The conserved sequence GxGxxP (127-132), comprising the loop between Nβ1 and the N-terminus of Nα1, probably binds the diphosphate bridge in NADH (*46*). The adenine moiety is expected to be positioned between the N-terminus of Nα4 and the loop preceding Nα3 (18,19,43), facing away from the flavin-binding domain.

Structural Implications for Electron Transfer. Ferredoxin-NADP reductases are a remarkable family of proteins that can transfer electrons from ferredoxin to $NAD(P)^+$, or in the reverse direction through a bound flavin cofactor. The direction of electron transfer is determined by the redox potentials of the cofactors, which are modulated by the surrounding protein (*47*). Redox potentials of FAD in MMOR are pH dependent (20,48), meaning that charged residues within MMOR modulate redox potential.

Phe245 (F342 in MMOR) is a conserved aromatic residue proposed in other proteins to act as a conformational gate regulating access of the nicotinamide moiety of NADH to the isoalloxazine ring (*19*). In the solution structure of the reduced protein, Phe245 is approximately 3.0 Å away from the *re*-face of FAD.

Direct evidence for these interactions is observed in long mixing time (180 ms) $^{1}H,^{15}N$ NOESY spectra of perdeuterated, ^{15}N labeled protein with protonated phenylalanine side chains. For the reduced form of MMOR, it is expected that this gate should block additional reduction by preventing binding of NADH, as well as stopping back electron transfer to oxidized NAD^+ by inducing its dissociation. Stopped flow experiments on both MMOR (*48*) and MMOR-FAD (*20*) give rate constants of 350 s^{-1} for a step after NADH binding prior to formation of a charge transfer complex between NADH and FAD. Based on our structure and the suggested role of Phe245 as a conformational gate, we propose that the gating movement of Phe245 and the concomitant displacement of the protein backbone are responsible for this observed rate constant for conversion of the initial Michaelis complex to the observed CT1 intermediate. In full length MMOR, electron transfer from the FAD cofactor to the [2Fe-2S] cluster occurs with a rate constant of 90 s^{-1}, while NAD^+ simultaneously dissociates from MMOR (*48*). Kinetics data from MMOR-FAD alone measure this rate constant for dissociation to be 89 s^{-1} without electron transfer (*20*). Thus additional conformational changes in the protein as a result of NAD^+ dissociation appear to be responsible for regulating electron transfer.

Conclusions We have solved the solution structure of the reduced FAD and NADH binding domains of MMOR by NMR spectroscopy. The results provide important structural information for the FAD and NADH binding domains in a reductase component of soluble MMO. Based on sequence homology, other sMMO reductases are expected to display similar protein folds. The structure of these domains is closely related

to those available for other members of the FNR family, whereas the FAD cofactor is found in an unprecedented extended conformation. Information gathered from these results, together with the previously determined structure of MMOR-Fd (17), will facilitate solution of the full-length MMOR structure and ultimately allow a greater understanding of the mechanism of electron transfer within sMMO.

Acknowledgment

We thank G. Heffron for technical assistance and V. M. Gelev for synthesis of [3-^{13}C]-α-ketobutyrate and [3,3'-^{13}C]-α-ketoisovalerate. Thank you to J. Müller for preparing figures 6, 7 and 8 and for assistance in writing, and to J. Gross for reviewing and helpful suggestions

References

1. Merkx, M., Kopp, D. A., Sazinsky, M. H., Blazyk, J. L., Müller, J., and Lippard, S. J. (2001) *Angew. Chem. Int. Ed.* **40**, 2782-2807
2. Que, L., Jr., and Dong, Y. (1996) *Acc. Chem. Res.* **29**, 190-196
3. Liu, K. E., and Lippard, S. J. (1995) *Adv. Inorg. Chem.* **42**, 263-289
4. Wallar, B. J., and Lipscomb, J. D. (1996) *Chem. Rev.* **96**, 2625-2658
5. Higgins, I. J., Best, D. J., and Hammond, R. C. (1980) *Nature* **286**, 561-564
6. Fox, B. G., Borneman, J. G., Wackett, L. P., and Lipscomb, J. D. (1990) *Biochemistry* **29**, 6419-6427
7. Colby, J., and Dalton, H. (1978) *Biochem. J.* **171**, 461-468
8. Stainthorpe, A. C., Lees, V., Salmond, G. P., Dalton, H., and Murrell, J. C. (1990) *Gene* **91**, 27-34
9. Merkx, M., and Lippard, S. J. (2002) *J. Biol. Chem.* **277**, 5858-5865
10. Rosenzweig, A. C., Frederick, C. A., Lippard, S. J., and Nordlund, P. (1993) *Nature* **366**, 537-543
11. Rosenzweig, A. C., Brandstetter, H., Whittington, D. A., Nordlund, P., Lippard, S. J., and Frederick, C. A. (1997) *Proteins* **29**, 141-152
12. Whittington, D. A., Rosenzweig, A. C., Frederick, C. A., and Lippard, S. J. (2001) *Biochemistry* **40**, 3476-3482
13. Whittington, D. A., and Lippard, S. J. (2001) *J. Am. Chem. Soc.* **123**, 827-838
14. Elango, N., Radhakrishnan, R., Froland, W. A., Wallar, B. J., Earhart, C. A., Lipscomb, J. D., and Ohlendorf, D. H. (1997) *Protein Sci.* **6**, 556-568
15. Walters, K. J., Gassner, G. T., Lippard, S. J., and Wagner, G. (1999) *Proc. Natl. Acad. Sci. U.S.A.* **96**, 7877-7882

16. Chang, S. L., Wallar, B. J., Lipscomb, J. D., and Mayo, K. H. (1999) *Biochemistry* **38**, 5799-5812

17. Müller, J., Lugovskoy, A. A., Wagner, G., and Lippard, S. J. (2002) *Biochemistry* **41**, 42-51

18. Correll, C. C., Batie, C. J., Ballou, D. P., and Ludwig, M. L. (1992) *Science* **258**, 1604-1610

19. Karlsson, A., Beharry, Z. M., Matthew Eby, D., Coulter, E. D., Neidle, E. L., Kurtz, D. M., Jr., Eklund, H., and Ramaswamy, S. (2002) *J. Mol. Biol.* **318**, 261-272

20. Blazyk, J. L., and Lippard, S. J. (2002) *Biochemistry* **41**, 15780-15794

21. Gross, J. D., Gelev, V. M., and Wagner, G. (2003) *J. Biomol. NMR* **25**, 235-242

22. Hajduk, P. J., Augeri, D. J., Mack, J., Mendoza, R., Yang, J., Betz, S. F., and Fesik, S. W. (2000) *J. Am. Chem. Soc.* **122**, 7898-7904

23. Ferentz, A. E., and Wagner, G. (2000) *Q. Rev. Biophys.* **33**, 29-65

24. Neri, D., Szyperski, T., Otting, G., Senn, H., and Wüthrich, K. (1989) *Biochemistry* **28**, 7510-7516

25. Güntert, P., Dötsch, V., Wider, G., and Wüthrich, K. (1992) *J. Biomol. NMR* **2**, 619-629

26. Bartels, C., Xia, T.-H., Billeter, M., Güntert, P., and Wüthrich, K. (1995) *J. Biomol. NMR* **5**, 1-10

27. Cornilescu, G., Delaglio, F., and Bax, A. (1999) *J. Biomol. NMR* **13**, 289-302

28. Güntert, P., Mumenthaler, C., and Wüthrich, K. (1997) *J. Mol. Biol.* **273**, 283-298

29. Güntert, P., Braun, W., and Wüthrich, K. (1991) *J. Mol. Biol.* **217**, 517-530

30. Brünger, A. T. (1992) *X-PLOR manual 3.1: A system for X-ray crystallography and NMR*, Yale University Press, New Haven, CT

31. Kleywegt, J. T. (1995) *CCP/ESF-EACBM Newsletter on Protein Crystallography* **31**, 45-50

32. Sridhar Prasad, G., Kresge, N., Muhlberg, A. B., Shaw, A., Jung, Y. S., Burgess, B. K., and Stout, C. D. (1998) *Protein Sci.* **7**, 2541-2549

33. Humphrey, W., Dalke, A., and Schulten, K. S. (1996) *J. Mol. Graphics* **14**, 33-38

34. Koradi, R., Billeter, M., and Wüthrich, K. (1996) *J. Mol. Graphics* **14**, 51-55, 29-32

35. Chou, J. J., Matsuo, H., Duan, H., and Wagner, G. (1998) *Cell* **94**, 171-180

36. Wishart, D. S., and Sykes, B. D. (1994) *J. Biomol. NMR* **4**, 171-180

37. Fleischmann, G., Lederer, F., Muller, F., Bacher, A., and Rüterjans, H. (2000) *Eur. J. Biochem.* **267**, 5156-5167

38. Griffin, K. J., Degala, G. D., Eisenreich, W., Müller, F., Bacher, A., and Frerman, F. E. (1998) *Eur. J. Biochem.* **255**, 125-132

39. Rüterjans, H., Fleischmann, G., Knauf, M., Löhr, F., Blümel, M., Lederer, F., Mayhew, S. G., and Müller, F. (1996) *Biochem. Soc. Trans.* **24**, 116-121

40. Shallop, A. J., Gaffney, B. L., and Jones, R. A. (2003) *J. Org. Chem.* **68**, 8657-8661

41. Ingelman, M., Bianchi, V., and Eklund, H. (1997) *J. Mol. Biol.* **268**, 147-157

42. Bruns, C. M., and Karplus, P. A. (1995) *J. Mol. Biol.* **247**, 125-145

43. Karplus, P. A., Daniels, M. J., and Herriott, J. R. (1991) *Science* **251**, 60-66

44. Serre, L., Vellieux, F. M., Medina, M., Gómez-Moreno, C., Fontecilla-Camps, J. C., and Frey, M. (1996) *J. Mol. Biol.* **263**, 20-39

45. Arakaki, A. K., Orellano, E. G., Calcaterra, N. B., Ottado, J., and Ceccarelli, E. A. (2001) *J. Biol. Chem.* **276**, 44419-44426

46. Correll, C. C., Ludwig, M. L., Bruns, C. M., and Karplus, P. A. (1993) *Protein Sci.* **2**, 2112-2133

47. Carrillo, N., and Ceccarelli, E. A. (2003) *Eur. J. Biochem.* **270**, 1900-1915

48. Kopp, D. A., Gassner, G. T., Blazyk, J. L., and Lippard, S. J. (2001) *Biochemistry* **40**, 14932-14941

49. Coufal, D. E., Blazyk, J. L., Whittington, D. A., Wu, W. W., Rosenzweig, A. C., and Lippard, S. J. (2000) *Eur. J. Biochem.* **267**, 2174-2185

50. Shigematsu, T., Hanada, S., Eguchi, M., Kamagata, Y., Kanagawa, T., and Kurane, R. (1999) *Appl. Environ. Microbiol.* **65**, 5198-5206

51. Fox, B. G., Liu, Y., Dege, J. E., and Lipscomb, J. D. (1991) *J. Biol. Chem.* **266**, 540-550

52. Cardy, D. L., Laidler, V., Salmond, G. P., and Murrell, J. C. (1991) *Arch. Microbiol.* **156**, 477-483

53. McDonald, I. R., Uchiyama, H., Kambe, S., Yagi, O., and Murrell, J. C. (1997) *Appl. Environ. Microbiol.* **63**, 1898-1904

54. Grosse, S., Laramee, L., Wendlandt, K. D., McDonald, I. R., Miguez, C. B., and Kleber, H. P. (1999) *Appl. Environ. Microbiol.* **65**, 3929-3935

55. Hall, T. A. (1999) *Nucl. Acids Sym. Ser.* **41**, 95-98

56. Nicholls, A., and Honig, B. (1990) *J. Comput. Chem.* **12**, 435-445

Table 1. Statistics for the MMOR-FAD Solution Structure

NOE distance constraints	3150
Intra-residue	1559
Sequential ($\|i-j\| = 1$)	671
Medium range ($\|i-j\| \leq 4$)	239
i, i+2	92
i, i+3	100
i, i+4	47
Long Range ($\|i-j\| \geq 5$)	434
Methyl constraints	247
H bond constraints	172
Dihedral angle constraints [a]	331
Average ensemble RMSD:	
FAD domain (10-111)	0.89 Å
NADH domain (113-250)	0.84 Å
Backbone (10-250)	0.98 Å
Procheck Analysis (percent)	
Most favored	90.2[b], 67.2[c]
Additional allowed	8.3[b], 21.1[c]
Generously allowed	1.0[b], 8.7[c]
Disallowed region	0.4[b], 3.0[c]

[a] Dihedral angle constraints as obtained with TALOS (*27*) or generated using DYANA (*28*) based on NOE constraints.
[b] Regular secondary structure
[c] Structured Region (residues 10-251)

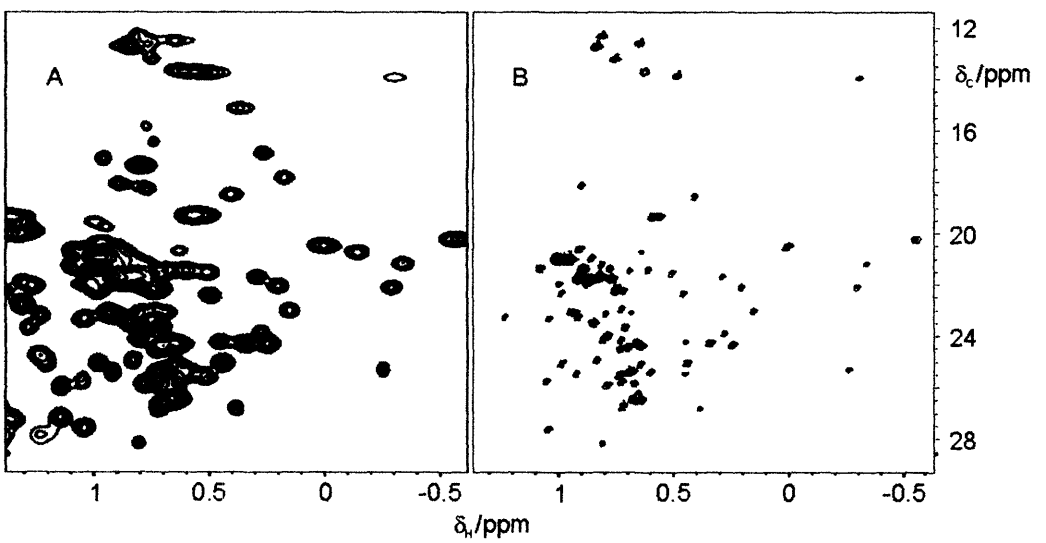

FIGURE 1-1. The aliphatic region of ^{13}C, ^{1}H HSQC spectra of MMOR–FAD for (A) uniformly ^{13}C labeled MMOR–FAD (spectrum recorded on 500 MHz Bruker NMR spectrometer with cryoprobe for 1 mM protein sample) and (B) ^{13}C terminal methyl (ILV) labeled MMOR–FAD (0.6 mM protein sample, spectrum recorded on 600 MHz Bruker NMR spectrometer).

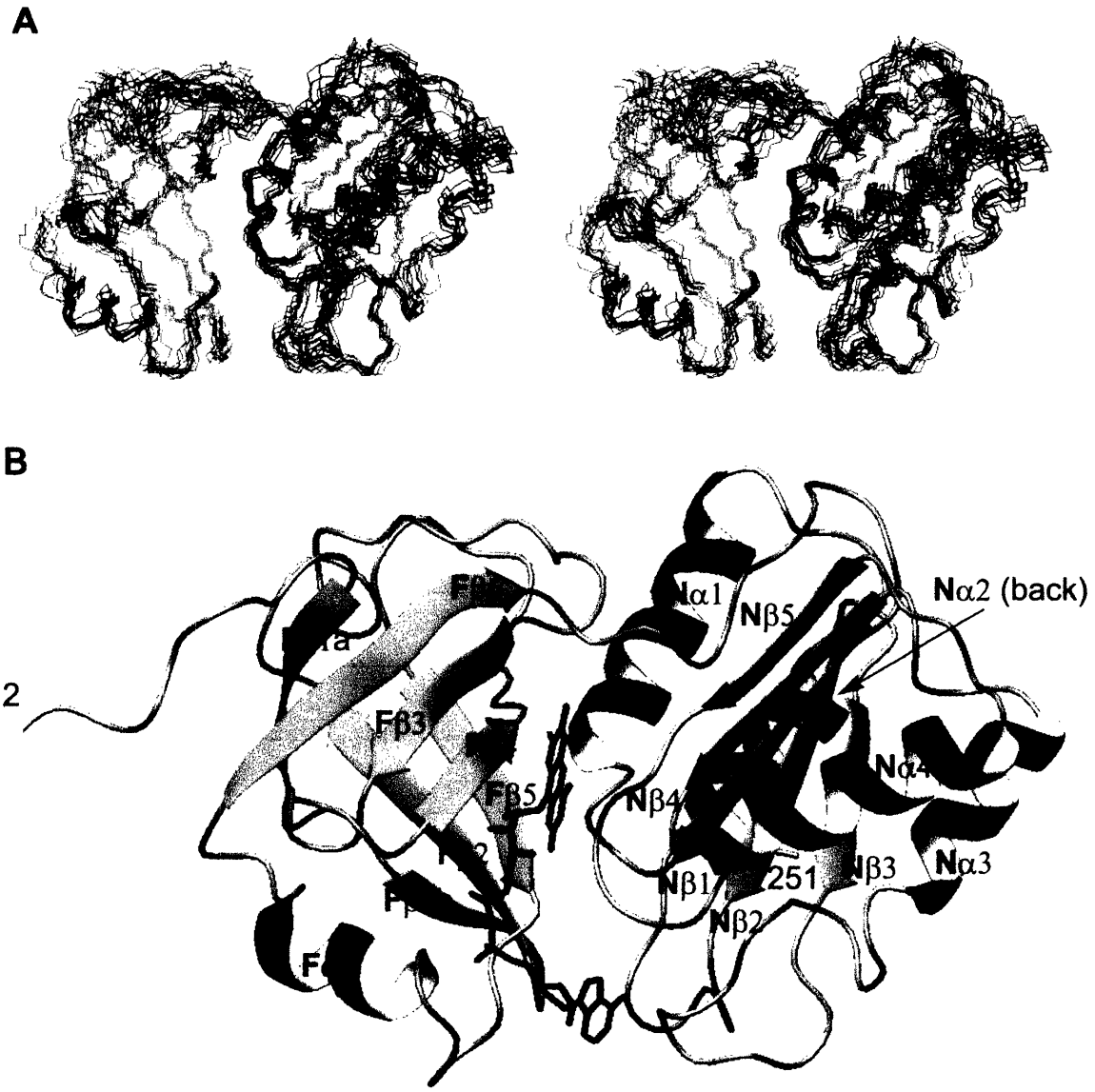

FIGURE 1-2. Solution structure of the FAD- and NADH- binding domains of MMOR. (A) The backbone atoms (N,Cα,C) of the 10 lowest energy NMR-derived structures are displayed in stereo view (residues 10-251). Secondary structural elements are shown colored in blue (β sheet) and red (α helix). This figure was created by superimposing backbone atoms for residues 10-250 using MOLMOL (34). (B) Ribbon diagram and nomenclature of FAD- and NADH-domains, with bound FAD cofactor shown in blue at the interface between the two domains.

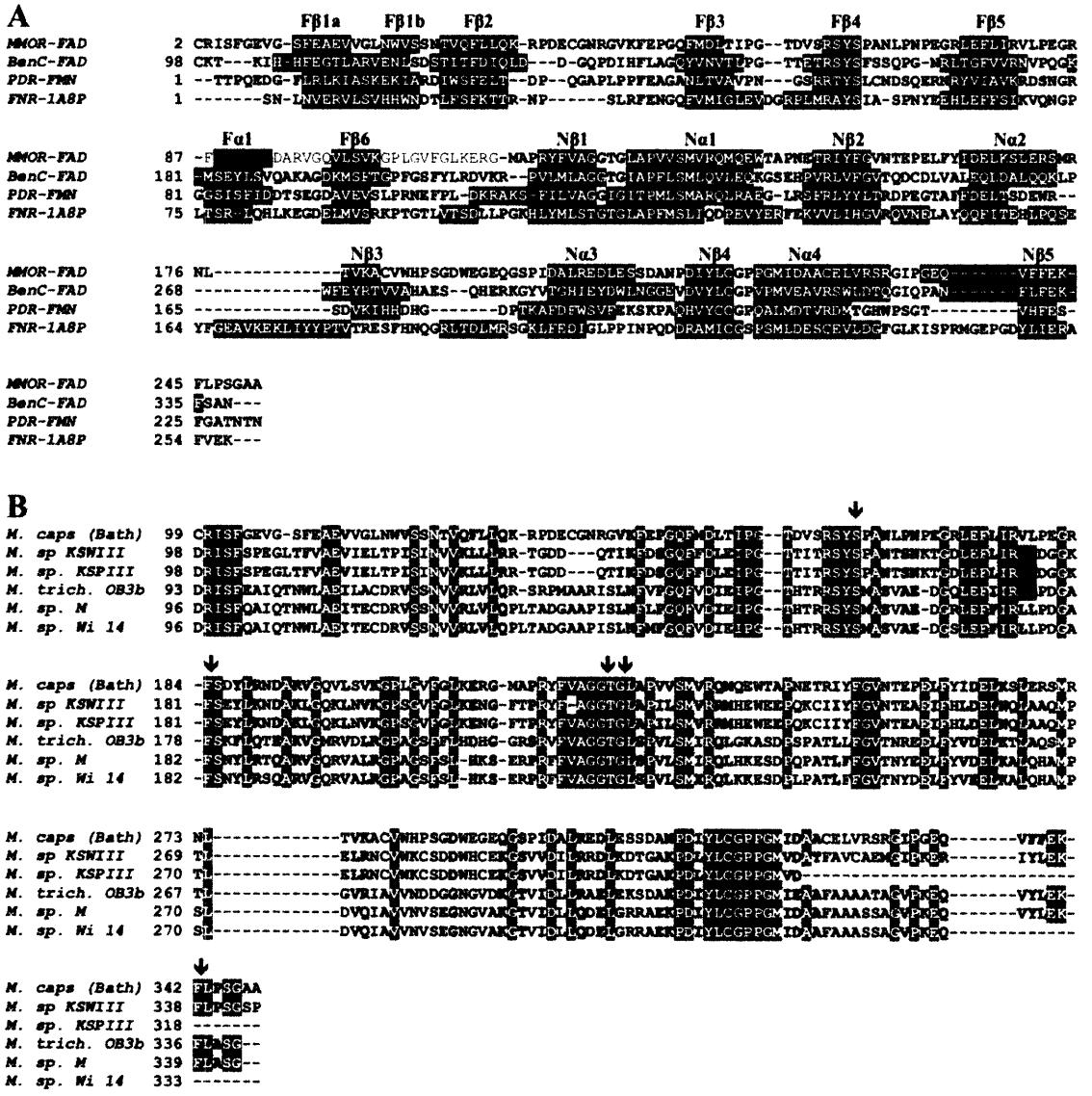

FIGURE 1-3. Sequence alignments of (A) FAD and NAD(P)H binding domain secondary structure of MMOR with benzoate-1,2-dioxygenase reductase (BenC, PDB code 1KRH) (*19*), phthalate dioxygenase reductase (PDR, PDB code 2PIA) (*18*), and NADPH:ferredoxin reductase (FdR, PDB code 1A8P) (32). Secondary structural elements are highlighted in red (α helices) or cyan (β sheets). (B) Sequence alignments of the FAD and NADH binding domains of the reductases in soluble MMO from methanotrophs *M. capsulatus* (Bath) (8,49), *Methylomonas* sp. strains KSWIII and KSPIII (*50*), *Methylosinus trichosporium* OB3b (51,52), *Methylocystis* sp. strain M (*53*), and *Methylocystis* sp. strain Wi 14 (*54*). Identical residues are highlighted in dark green, whereas similar residues are in light green. Residues marked with arrows are discussed in the text as being involved in FAD binding. Figures were made using BioEdit (*55*).

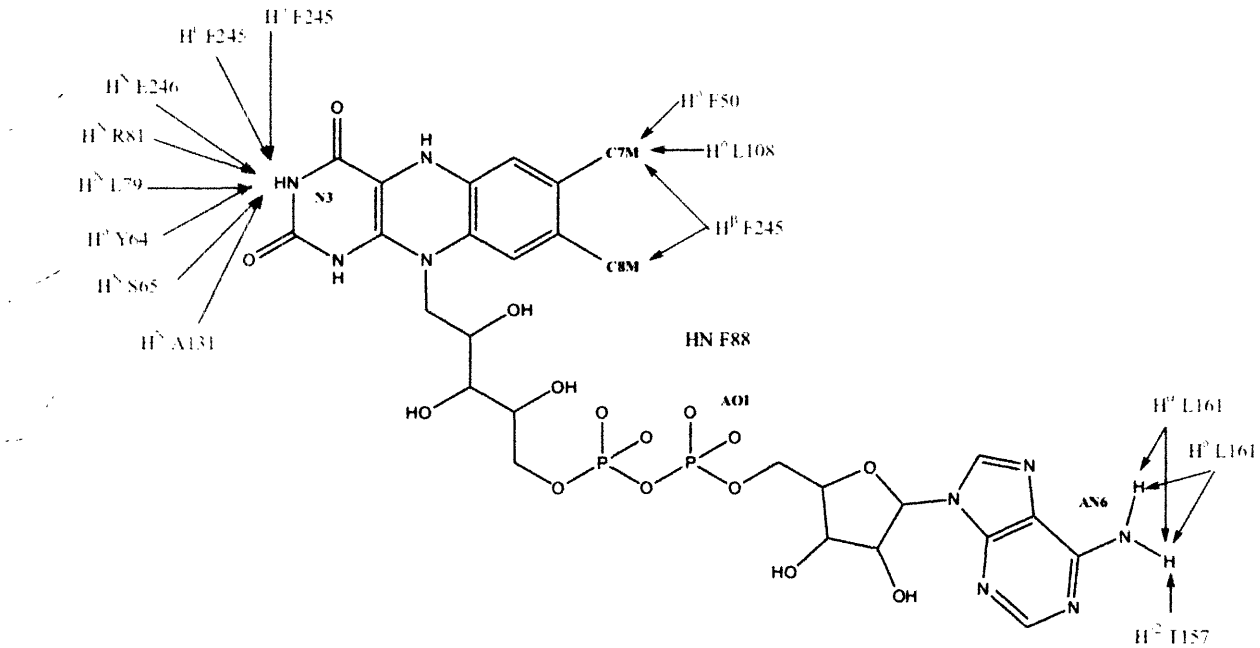

FIGURE 1-4. Intermolecular NOEs and hydrogen bonds between the protein and FAD cofactor. FAD is shown in black, with atom names listed, and blue arrows indicate intermolecular NOEs. The hydrogen bond between Phe88 and the phosphate oxygen AO1 is shown as a cyan dashed line.

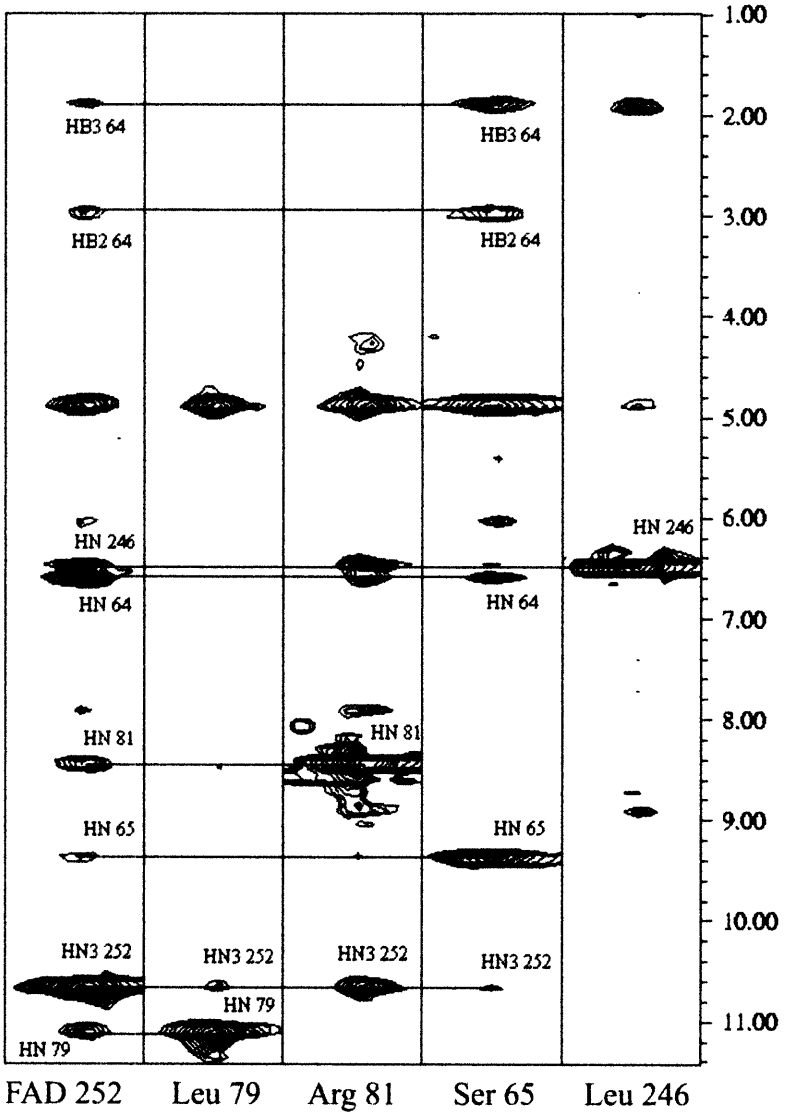

FIGURE 1-5. Selected strips from the 180 ms mixing time ^{15}N NOESY-HSQC spectrum with protonated Y and W residues in ^{15}N, ^{2}H labeled protein. FAD252 has a peak for HN3 in the first strip, with crosspeaks to $H^{\beta 2}$ and $H^{\beta 3}$ of Tyr64, HN of Ser65, HN of Leu79, HN of Arg81 and HN of Leu246. The corresponding strips show the amide peaks and their crosspeaks to FAD252. These interactions are direct evidence for FAD binding in MMOR–FAD.

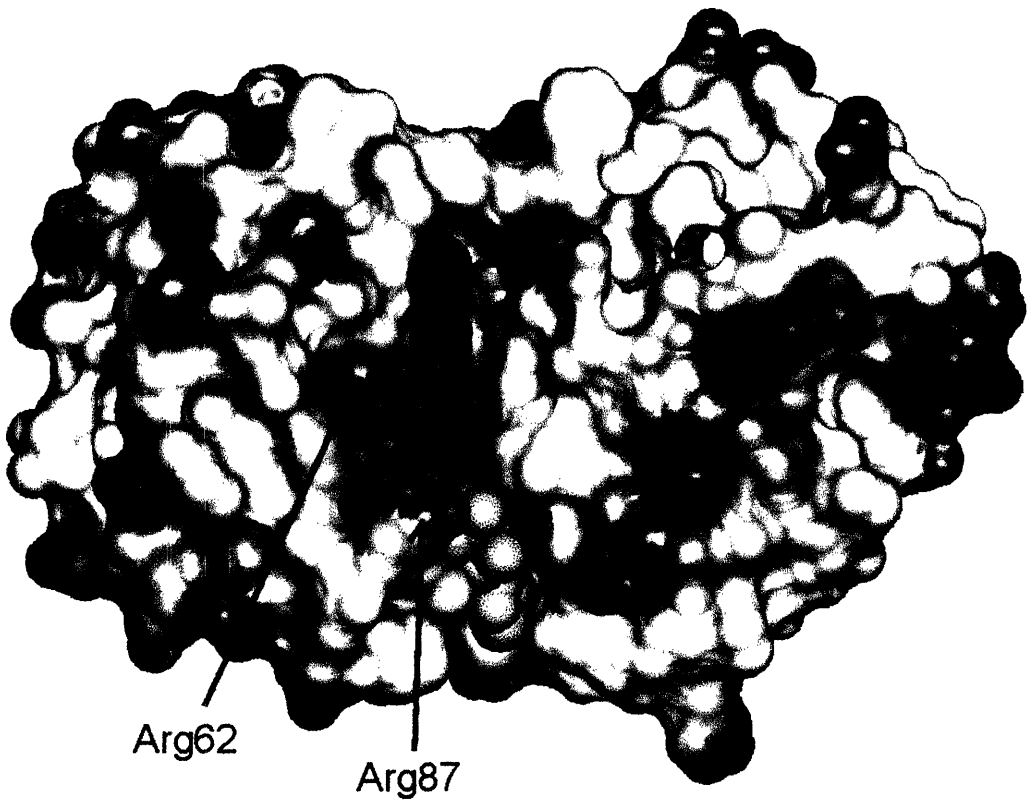

FIGURE 1-6. Electrostatic surface plot of the MMOR–FAD protein core (residues 11-251), revealing that the FAD cofactor is located in a cleft between the two domains. Red and blue represent negative and positive partial charges, respectively. The FAD prosthetic group is shown in green (dark green: riboflavin, green: phosphate groups, light green: adenosine). The positive charge provided by arginine side chains of the FAD-binding domain stabilizing the phosphate groups is clearly discernible. This figure was generated with an algorithm (*56*) implemented in MolMol using relative dielectric constants of 3 and 80 for the protein and surrounding water, respectively. A box extending 10 away from the protein in each direction was used when calculating the potential.

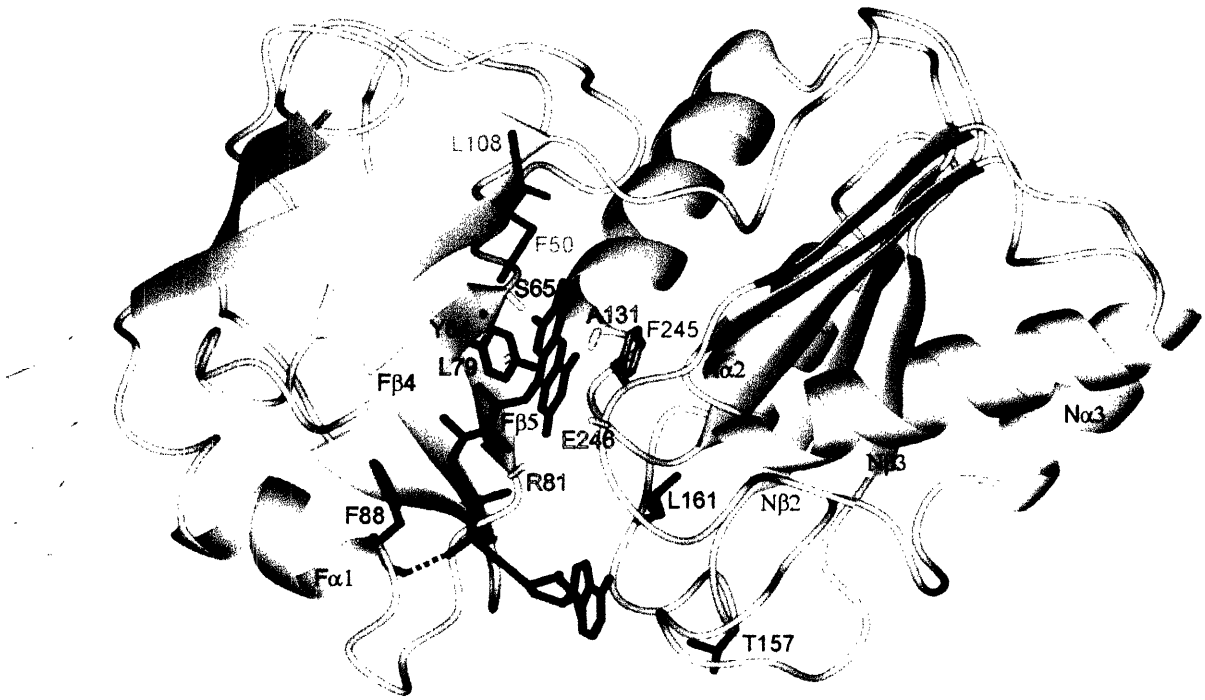

FIGURE 1-7. Experimentally observed contacts between FAD cofactor and protein. FAD is in blue, the residues Phe245, Tyr64 and Phe88 as discussed in the text are shown in orange, red, and black, respectively. The hydrogen bond pointing from the Phe88 amide proton to the AMP phosphate group is also shown. Amino acids with observed contacts to the adenine-N6 group are in dark green, those with contacts to the flavin methyl groups are in green. N-H bonds are displayed in yellow for residues with short contacts to the isoalloxazine N3 amide proton.

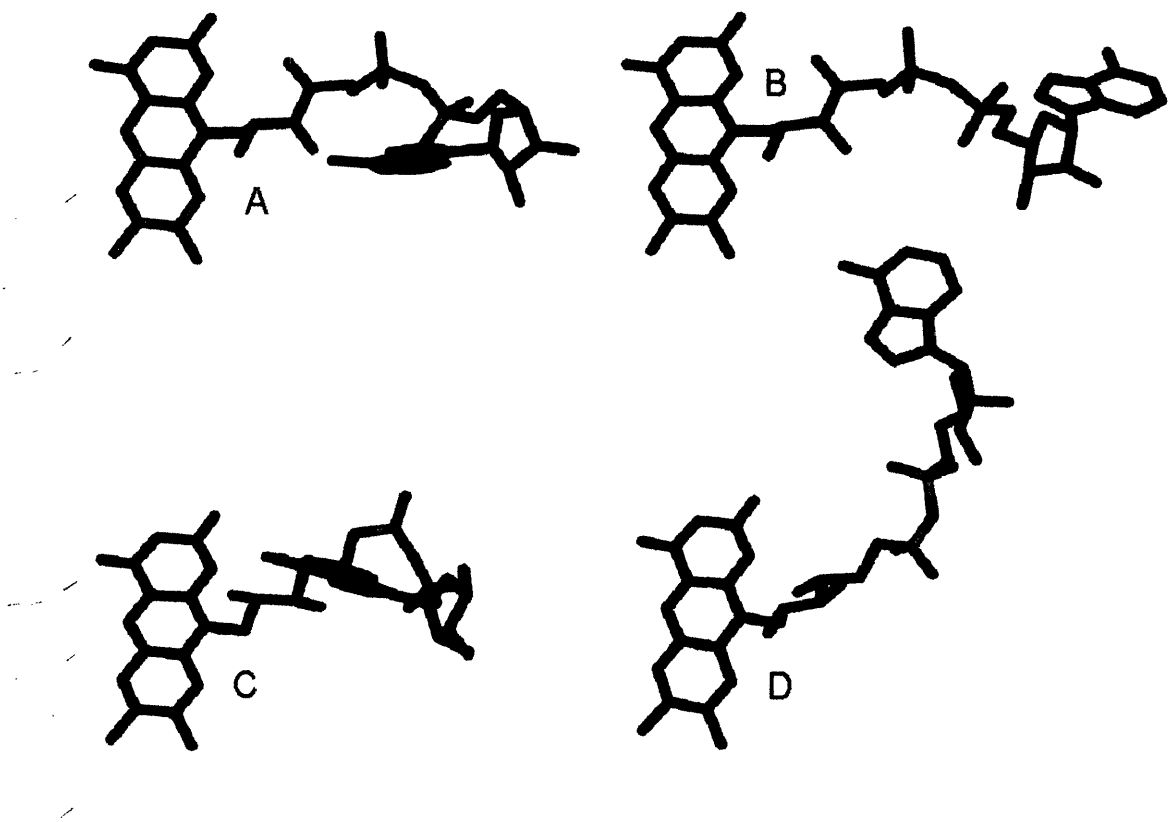

FIGURE 1-8. Comparison of the conformation of the FAD cofactor in different protein structures. A: BenC, B: spinach FNR, C: FdR, D: MMOR–FAD.

Chapter 2: Investigation of the Role of Phe 342 as a Conformational Gate for Electron Transfer in MMOR

Introduction

Methanotrophic bacteria utilize methane as a primary carbon and energy source, a remarkable feat given that the C–H bond in methane is one of the most stable found in nature with an energy of 104 kcal/mol. The first step in the pathway of carbon uptake is the conversion of methane to methanol, catalyzed by the multi-enzyme methane monooxygenase (MMO) system and shown in equation 1 (1-4).

$$CH_4 + NADH + H^+ + O_2 \rightarrow CH_3OH + NAD^+ + H_2O \qquad (1)$$

The MMO system is found in both particulate and soluble forms, the former being a copper-containing oxygenase whereas the latter is expressed under low copper conditions. Soluble MMO from *Methylococcus capsulatus* (Bath) consists of four enzymes: a 251 kDa $\alpha_2\beta_2\gamma_2$ hydroxylase component containing a diiron site in each α subunit responsible for O_2 activation and hydroxylation of methane, a 15.9 kDa regulatory protein MMOB, the 38.7 kDa reductase (MMOR) which transfers electrons from NADH into the diiron site in the hydroxylase, and a fourth 12 kDa component (MMOD) of undetermined function (5-7). Structures for MMOH in various redox states were solved by X-ray crystallography (8-12), and NMR spectroscopy was used to solve the structures of MMOB (13,14), and both the ferredoxin (15) and flavin-binding (16) domains of MMOR in the reduced state.

The reductase component is structurally homologous to other dioxygenase reductase proteins, most notably benzoate-1,2-dioxygenase reductase, or BenC (17), and phthalate dioxygenase reductase, PDR (18), both structures having been

solved previously by X-ray crystallography. These proteins are all members of the ferredoxin-$NADP^+$ reductase (FNR) subfamily, one subset of the flavodoxin family. This subfamily is named for the ferredoxin-$NADP^+$ reductases, part of the photosynthetic pathway. These proteins utilize a conserved flavin-binding domain with a six-stranded antiparallel beta barrel structure having a single alpha helix at one end, together with a conserved pyridine nucleotide-binding domain containing a five-stranded parallel beta sheet surrounded by 4-9 alpha helices. FAD or FMN is bound along the interface between the two domains. Ferredoxin-$NADP^+$ reductases transfer electrons from separate ferredoxin molecules to reduce $NADP^+$ to NADPH via the flavin cofactor. The linked monooxygenase and dioxygenase reductases MMOR, PDR, and BenC have the ferredoxin domain attached to the N- or C- terminus of the FNR protein and transfer electrons in the opposite direction, using NADH to reduce the ferredoxin domain. Figure 2-1 diagrams the various links between domains of these proteins. Modulation of redox potentials of bound cofactors by surrounding protein enables this basic scaffold to transfer electrons in both directions (19).

One feature of the FNR subfamily is a conserved C-terminal aromatic residue located spatially near the re-face of the isoalloxazine ring. This residue is a conserved tyrosine for ferredoxin-$NADP^+$ reductases, whereas phenylalanine is in this position for proteins like MMOR and BenC. This tyrosine residue has been proposed to play a catalytic role for FNR by acting as a conformational gate, as well as modulating FAD redox potentials and formation of the ternary complex with ferredoxin (20). A similar conformational role for the C-terminal phenylalanine in MMOR, PDR, BenC and in nitric oxide synthases has been

proposed based on crystal and solution structures of these proteins (16-18,21). Figure 2-2 shows Phe 245 in the reduced MMOR-FAD domain with its side chain parallel to the flavin ring in the purported nicotinamide binding site for NADH. In this chapter, mutants of C-terminal phenylalanine residue 342 in the full-length reductase or Phe 245 in the MMOR-FAD flavin domain were created to investigate the role of this amino acid.

Materials and Methods

Site-Directed Mutagenesis. The QuikChange II kit (Stratagene) was used for mutagenesis. Mutants of the MMOR-FAD domain protein were constructed using a pET21(+) plasmid containing the recombinant gene for MMOR-FAD, pFAD21. Full-length MMOR mutants were created with recombinant plasmid pRED24, a pET24(+) construct containing the *mmoC* gene. The 31-mer primers were purchased from Invitrogen and were created using a Stratagene toolkit program to optimize length and melting temperature of primers for use in the QuikChange protocol. For the F245Y and F342Y mutants, primer sequences 5'GGTCTTCTTCGAAAAATACCTGCCGTCCGGG 3' and 5'-CCCGGACGGC AGGTATTTTTCGAAGAAGACC-3', with mutation sites underlined, were used. Corresponding primers for F245A/F342A and F245L/F342L contained mutations GCC/GGC or CTC/GAG in the underlined regions of the previous sense and antisense primers, respectively. Mutants were constructed by using 15-20 12 or 15 min PCR cycles with PfuTurbo DNA polymerase. The resulting plasmid mixture was treated with restriction enzyme DpnI to remove nonmutated template DNA and transformed into supercompetent XL-1 Blue cells. Resulting

colonies were grown in 5 mL cultures overnight, and plasmids were isolated from these cells using a Qiaprep spin miniprep kit (Qiagen). The plasmids obtained were sequenced by the MIT Biopolymers facility to verify the presence of the appropriate gene mutation, and BL21(DE3) cells were transformed with mutant-containing plasmids.

Expression and Purification. MMOR-FAD domain protein mutants were grown in 1L cultures of LB media with 100 mM ampicillin added. Cells were grown to an OD_{600} of 0.6, then induced with 1 mM IPTG and induced for 3 h. Cells were centrifuged and lysed by sonication. Crude protein was purified as described previously (22). Full-length MMOR mutants were grown in M9 minimal media with 30 mg/L kanamycin to OD_{600} of 0.6, followed by a 6 h induction period with 0.1 mM IPTG. Cells were centrifuged to harvest and lysed by sonication in the presence of 500 μM $MgCl_2$, 10 μL DNase I, 12.5 mg Pefabloc protease inhibitor and approximately 100 mg PMSF in 20 mM Tris buffer, pH 7.2 with 50 mM NaCl and 8 mM sodium thioglycolate. MMOR mutants were purified as described previously (23). Purity of isolated mutant proteins was verified by SDS-PAGE with 4-20% Tris-HCl gradient gels (BioRad). Purified protein was desalted and exchanged into 25 mM MOPS, pH 7.0 with 1 mM DTT for storage at –80 °C.

Characterization of Mutants. UV-visible spectra for mutants were recorded on a HP 8453 spectrophotometer. Spectra were recorded for the oxidized protein in 25 mM MOPS buffer, pH 7.0. Flavin content was determined by comparing the ratio of absorbances at 270 and 458 nm, with a value of ~6.7 corresponding to 1 FAD cofactor per protein.

Iron content for the full-length proteins was determined by assaying reduced Fe^{2+} with ferrozine. Iron was reduced to Fe^{2+} by addition of ascorbic acid, and

protein was precipitated by using 0.7 M trichloroacetic acid. To the resulting supernatant was added ferrozine and the reaction was taken to completion, approximately 20 min. The concentration of the colored complex was measured at 562 nm on a UV-vis spectrophotometer. Protein samples were compared to a standard curve to determine the iron content of the mutant reductase forms.

Stopped-Flow Experiments. All experiments were performed on a Hi-Tech model SF-61 DX2 instrument with a photomultiplier and tungsten lamp for single wavelength mode or diode array detection with a 75 W xenon arc lamp. Syringes and the flow line were made anaerobic by filling with 25 mM MOPS buffer, pH 7.0 containing approximately 5 mM sodium dithionite for approximately 30-45 min, followed by a flush of the system with anaerobic 25 mM MOPS buffer, pH 7.0. All buffers and NADH solutions were made anaerobic by bubbling nitrogen through the solution for at least 30 min. Protein samples were made anaerobic by running 12-15 cycles of vacuum/nitrogen gas exchange. Samples were run at 4.0 °C, and all data were recorded with a logarithmic time base. Data from single wavelength absorbance experiments were fit using the program KinetAsyst v. 2.0 (Hi-Tech, Ltd).

Results

Characterization of MMOR-FAD mutants. All mutants of MMOR-FAD were expressed as bright yellow proteins with elution profiles identical to that of wild-type MMOR-FAD domain protein. Purified mutants had approximate molecular weights of 27,000 kDa, as determined by SDS-PAGE gel electrophoresis. A scan of an SDS-PAGE gel containing the purified mutants is shown in Figure 2-3.

Absorbance spectra of wild-type protein and F245 mutant series are shown in Figure 2-4. There is a slight blue shift in the flavin peak at 396 nm compared to the wild type protein and mutants. The F245Y mutant has a maximum at 389 nm, whereas F245L is shifted to 387 nm and F245A has a maximum at 386 nm. The maxima at 270 nm and 458 nm found in the wild-type spectrum are unchanged in these mutants.

Characterization of MMOR mutants. The full-length MMOR mutants were expressed as dark brown proteins with elution profiles similar to that of wild-type MMOR-FAD. Both F342A and F342L mutants eluted prior to solubilized Fe-S clusters rather than after this band, as observed for wild-type protein. Purified F342Y and F342A MMOR had approximate molecular weights of 37,500 kDa, similar to that of wild-type MMOR, as shown in Figure 2-3. The F342L mutant precipitated at higher concentrations and resulted in a large smear in the SDS-PAGE gel. The iron content for all mutants was measured as 2.0 iron per protein, in good agreement with the value of 2.0 Fe/protein reported for full-length recombinant MMOR previously (23).

UV-visible absorbance spectra of the full-length mutants are shown in Figure 2-5. There is a shift in the maximum of the minor flavin peak from 396 nm in MMOR to 389 nm in F342Y, with more pronounced shifts for F342L and F342A at 384 nm and 382 nm, respectively. Additionally, the [2Fe-2S] peak observed in the oxidized MMOR at 338 nm is diminished in magnitude relative to the other visible peaks in F342Y. In the F342A and F342L absorbance spectra, this peak is no longer present.

Kinetic behavior of mutant reduction by NADH. Rate constants for the reduction of MMOR-FAD and MMOR mutants by NADH are summarized in Table 2-1.

Rate constants k_2 and k_3 (and k_4) were determined by fitting data traces at 725 or 740 nm, whereas rate constant k_1 was determined from analysis of fits at 625 nm with previously measured values of k_2, k_3 and k_4.

In MMOR-FAD, only three rate constants for electron transfer from NADH to FAD are observed, corresponding to the steps labeled in Scheme 2-1a (22). The first rate constant, k_1, corresponds NADH binding to a position for electron transfer to take place, forming charge transfer complex 1 (CT1). The second rate constant follows formation of charge transfer complex 2 (CT2), where electron transfer to the oxidized flavin takes place, forming the two electron reduced form of FAD, FAD_{hq}. The third rate constant measures decomposition of CT2, monitored at 725 nm, by dissociation of oxidized NAD^+ from MMOR-FAD. Figure 2-6 shows typical traces for wild-type MMOR-FAD and the three mutants at 458, 625 and 725 nm. Disappearance of the absorbance peak for oxidized flavin is followed at 458 nm, while FAD semiquinone formation and disappearance can be traced at 625 nm (24). Values for k_1 are half that of the wild-type rate constants for mutants F245Y and F245A, whereas this rate constant is unchanged for F245L. For mutant F245L there is virtually no decrease in k_2 compared to wild-type MMOR-FAD; this rate constant is slightly slower for F245Y, 132 s^{-1}, and about 50% of the native value for F245A. The difference in k_3 values is most striking for mutant F245A, being 6.1 s^{-1}, corresponding to a fifteen-fold decrease from wild-type activity. Rate constants measured for this third step are nearly identical for F245Y and F245L, 61 s^{-1} and 66 s^{-1}, respectively.

For full-length MMOR, a fourth kinetic step is required to fit data obtained at 625 nm, suggesting an additional step or pathway for electron transfer for decomposition of FAD semiquinone. In MMOR, this step has been measured to

have a rate constant of 25 s^{-1}. Values determined for the first rate constant in full-length mutants are roughly the same as k_1 for the MMOR-FAD mutants. The F342Y mutant has values for rate constants that are slightly lower than those of wild-type MMOR, and similar to rate constants measured for corresponding FAD domain mutant, F245Y. The full-length alanine mutant, F342A, displays values matching those measured for the FAD domain protein, with a k_4 rate constant three orders of magnitude slower than that of wild-type MMOR. The F342L mutant displays radically different behavior from wild-type MMOR in its semiquinone trace at 625 nm. Formation of semiquinone is followed by immediate decay, rather than by the slow decay seen in traces of MMOR and the other mutants in Figure 2-7. Rate constants for the F342L mutant from data fitting are not significantly different from that of wild-type MMOR, however.

Discussion

Comparison of mutants to wild-type proteins. Conservative mutations of the C-terminal phenylalanine in MMOR and its flavin binding domain result in proteins with no loss in cofactor content or major conformational changes. All mutants bind NADH and transfer electrons, thus allowing a comparison of their activities to that of the wild-type proteins. The slight spectral shift towards shorter wavelengths observed in the peak at 396 nm is observed in similar mutants of FNR from *Anabaena* (20). This shift, due to FAD bound in the protein, suggests that the binding environment around this cofactor becomes more hydrophobic with changes to smaller residues like alanine and leucine, or, it may be due to a change in interaction of the aromatic side chain with the flavin ring.

A small shift is also observed for the F245Y and F342Y mutants, but the effect is not as large as it is for alanine and leucine, not an unexpected result since the mutation of phenylalanine to tyrosine is very conservative.

There is a definite change in the kinetic behavior of both the F245 and F342 mutants, which have diminished rates compared to wild type MMOR and MMOR-FAD. The lowered rate constants observed for MMOR-FAD in mutants F245Y and F245L remain within the same order of magnitude as that of the wild-type protein. Full-length mutant F342Y also shows a decrease electron transfer rates, but this process still occurs on a similar time scale to that of the wild-type MMOR. The most dramatic slowing of electron transfer is observed in the F245A and F342A mutants, where the rate-limiting electron transfer step of 90 s^{-1} observed in both MMOR and MMOR-FAD is slowed to 6.2 s^{-1}, a fifteen-fold decrease in the rate constant. The rate of decay of CT2 observed at 725 nm in MMOR-FAD and at 740 nm in MMOR corresponds to dissociation of NAD^+ from the protein, along with simultaneous electron transfer from reduced FAD to the [2Fe-2S] cluster in MMOR to form the FAD semiquinone. The decrease in k_3 for the alanine mutants lends support to the postulated role of Phe342 as a conformational gate necessary to extrude oxidized NAD^+ rapidly to promote electron transfer to the ferredoxin domain of the reductase.

The kinetic behavior of F342L is intriguing. Although no significant difference in rate was observed for electron transfer in the FAD domain protein from wild-type, the full-length mutant shows some surprising behavior in the decay of semiquinone. Wild-type MMOR and both F342Y and F342A showed buildup of FAD_{sq} in the trace at 625 nm, followed by a slow decay occurring beyond the time scale measured in the experiment, indicating formation of FAD_{sq} resulting

from transfer of electrons to the [2Fe-2S] cluster. In F342L, however, a rapid decay of this complex is observed, suggesting alternate routes for this process that prevent electron transfer to the ferredoxin domain from occurring. There may be little driving force for electron transfer in this mutant, although the measured rates were similar to those of both wild-type MMOR and MMOR-FAD. Rapid back-electron transfer to the oxidized NAD^+ cofactor while still bound to MMOR may be another possible explanation. Redox potential measurements for the mutants are necessary to elucidate what occurs in this mutant.

Role of F342 as a conformational gate for electron transfer. The difference in electron transfer rates between the mutant FAD domain and wild-type proteins confirms that Phe 342 does indeed play a role in modulating electron transfer between NADH and the oxidized FAD. Surprisingly, the major effect is not in the first rate constant, which reflects movement the nicotinamide ring of NADH near the flavin ring, forming charge complex CT1 capable of electron transfer. This step was initially expected to be perturbed to the greatest degree by mutations of Phe 342, since it was anticipated that phenylalanine was physically blocking the nicotinamide binding site prior to NADH binding. Rather, the effect of this phenylalanine substitution is manifest in a large change for rate constant k_3, particularly for the alanine mutants. Loss of the large hydrophobic group retards dissociation of NAD^+ from the reduced flavin, thereby slowing electron transfer from the reduced flavin to the [2Fe-2S] cluster.

X-ray structures of oxidized FNR proteins reveal that the corresponding C-terminal tyrosine side chain blocking access of the $NADP^+$ nicotinamide ring to the flavin ring (25,26). Electron transfer in this system proceeds in the opposite

direction, thus, the fully reduced flavin must be formed prior to interaction with $NADP^+$ for electron transfer. Our mutant results suggest that phenylalanine is in a conformation that allows the nicotinamide ring to access the flavin ring for electron transfer, and that rate k_1 does not involve a conformational change requiring Phe342 to move out of the way. After reduction of the flavin has taken place, a conformational change in the protein moves the phenylalanine side chain into the nicotinamide binding site of NADH, pushing oxidized NAD^+ out of the way to prevent back electron transfer and allowing electrons to be transferred to reduce the ferredoxin cluster and ultimately the diiron site in MMOH.

Conclusions. Based on studies of this series of Phe 245 and 342 mutants, electron transfer from NADH to oxidized FAD is regulated by the action of Phe 342. Removal of large hydrophobic groups slows the rate of NAD^+ dissociation dramatically, as observed by the significant drop in rate constant k_3 for F245A and F342A. The rapid loss of semiquinone after reduction in the F342L mutant suggests that electron transfer to the ferredoxin domain can not occur because of another pathway for electron transfer, potentially implicating requirement of an aromatic interaction with the flavin ring to stabilize the semiquinone form of FAD to allow electron transfer. Redox potentials for cofactors in these mutants need to be measured to explain further these results and to verify that the change in ET rates is due to conformational restrictions rather than alterations in the driving force for electron transfer.

Acknowledgements

I would like to thank Jessica Blazyk and Dong Xu for helpful discussions and assistance in running the stopped-flow system and data fitting.

References

1. Merkx, M., Kopp, D. A., Sazinsky, M. H., Blazyk, J. L., Müller, J., and Lippard, S. J. (2001) *Angew. Chem. Int. Ed.* **40**, 2782-2807
2. Que Jr., L., and Dong, Y. (1996) *Acc. Chem. Res.* **29**, 190-196
3. Liu, K. E., and Lippard, S. J. (1995) *Adv. Inorg. Chem.* **42**, 263-289
4. Wallar, B. J., and Lipscomb, J. D. (1996) *Chem. Rev.* **96**, 2625-2658
5. Colby, J., and Dalton, H. (1978) *Biochem. J.* **171**, 461-468
6. Stainthorpe, A. C., Lees, V., Salmond, G. P., Dalton, H., and Murrell, J. C. (1990) *Gene* **91**, 27-34
7. Merkx, M., and Lippard, S. J. (2002) *J. Biol. Chem.* **277**, 5858-5865
8. Rosenzweig, A. C., Frederick, C. A., Lippard, S. J., and Nordlund, P. (1993) *Nature* **366**, 537-543
9. Rosenzweig, A. C., Brandstetter, H., Whittington, D. A., Nordlund, P., Lippard, S. J., and Frederick, C. A. (1997) *Proteins* **29**, 141-152
10. Whittington, D. A., and Lippard, S. J. (2001) *J. Am. Chem. Soc.* **123**, 827-838
11. Whittington, D. A., Sazinsky, M. H., and Lippard, S. J. (2001) *J. Am. Chem. Soc.* **123**, 1794-1795
12. Elango, N., Radhakrishnan, R., Froland, W. A., Wallar, B. J., Earhart, C. A., Lipscomb, J. D., and Ohlendorf, D. H. (1997) *Protein Sci.* **6**, 556-568
13. Chang, S. L., Wallar, B. J., Lipscomb, J. D., and Mayo, K. H. (1999) *Biochemistry* **38**, 5799-5812
14. Walters, K. J., Gassner, G. T., Lippard, S. J., and Wagner, G. (1999) *Proc. Natl. Acad. Sci.* **96**, 7877-7882
15. Müller, J., Lugovskoy, A. A., Wagner, G., and Lippard, S. J. (2002) *Biochemistry* **41**, 42-51

16. Chatwood, L. L., Müller, J., Gross, J. D., Wagner, G., and Lippard, S. J. (2004) *Biochemistry* in press.

17. Karlsson, A., Beharry, Z. M., Matthew Eby, D., Coulter, E. D., Neidle, E. L., Kurtz, D. M., Jr., Eklund, H., and Ramaswamy, S. (2002) *J. Mol. Biol.* **318**, 261-272

18. Correll, C. C., Batie, C. J., Ballou, D. P., and Ludwig, M. L. (1992) *Science* **258**, 1604-1610

19. Carrillo, N., and Ceccarelli, E. A. (2003) *Eur. J. Biochem.* **270**, 1900-1915

20. Nogués, I., Tejero, J., Hurley, J. K., Paladini, D., Frago, S., Tollin, G., Mayhew, S. G., Gómez-Moreno, C., Ceccarelli, E. A., Carrillo, N., and Medina, M. (2004) *Biochemistry* **43**, 6127-6137

21. Adak, S., Sharma, M., Meade, A. L., and Stuehr, D. J. (2002) *Proc. Natl. Acad. Sci.* **99**, 13516-13521

22. Blazyk, J. L., and Lippard, S. J. (2002) *Biochemistry* **41**, 15780-15794

23. Kopp, D. A., Gassner, G. T., Blazyk, J. L., and Lippard, S. J. (2001) *Biochemistry* **40**, 14932-14941

24. Gassner, G. T., and Lippard, S. J. (1999) *Biochemistry* **38**, 12768-12785

25. Hermoso, J. A., Mayoral, T., Faro, M., Gómez-Moreno, C., Sanz-Aparicio, J., and Medina, M. (2002) *J. Mol. Biol.* **319**, 1133-1142

26. Bruns, C. M., and Karplus, P. A. (1995) *J. Mol. Biol.* **247**, 125-145

Table 2-1: Kinetic parameters for MMOR-FAD and MMOR mutants

	k_1 (s^{-1})	k_2 (s^{-1})	k_3 (s^{-1})	k_4 (s^{-1})
MMOR-FAD				
Wild-type[a]	240 (20)	188 (7)	89 (4)	-
F245Y	150 (20)	132 (3)	61 (2)	-
F245A	110 (20)	92 (2)	6.1(2)	-
F245L	230 (40)	180 (10)	66 (8)	-
MMOR				
Wild-type[b]	350	193	90	29 (1)
F342Y	140 (20)	108 (3)	72 (2)	13 (1)
F342A	120 (10)	93 (2)	6.4 (1)	0.014 (4)
F342L	220 (30)	123 (2)	82 (3)	17 (2)

[a] As reported in ref. (22)
[b] Rate constants reported in ref. (23)

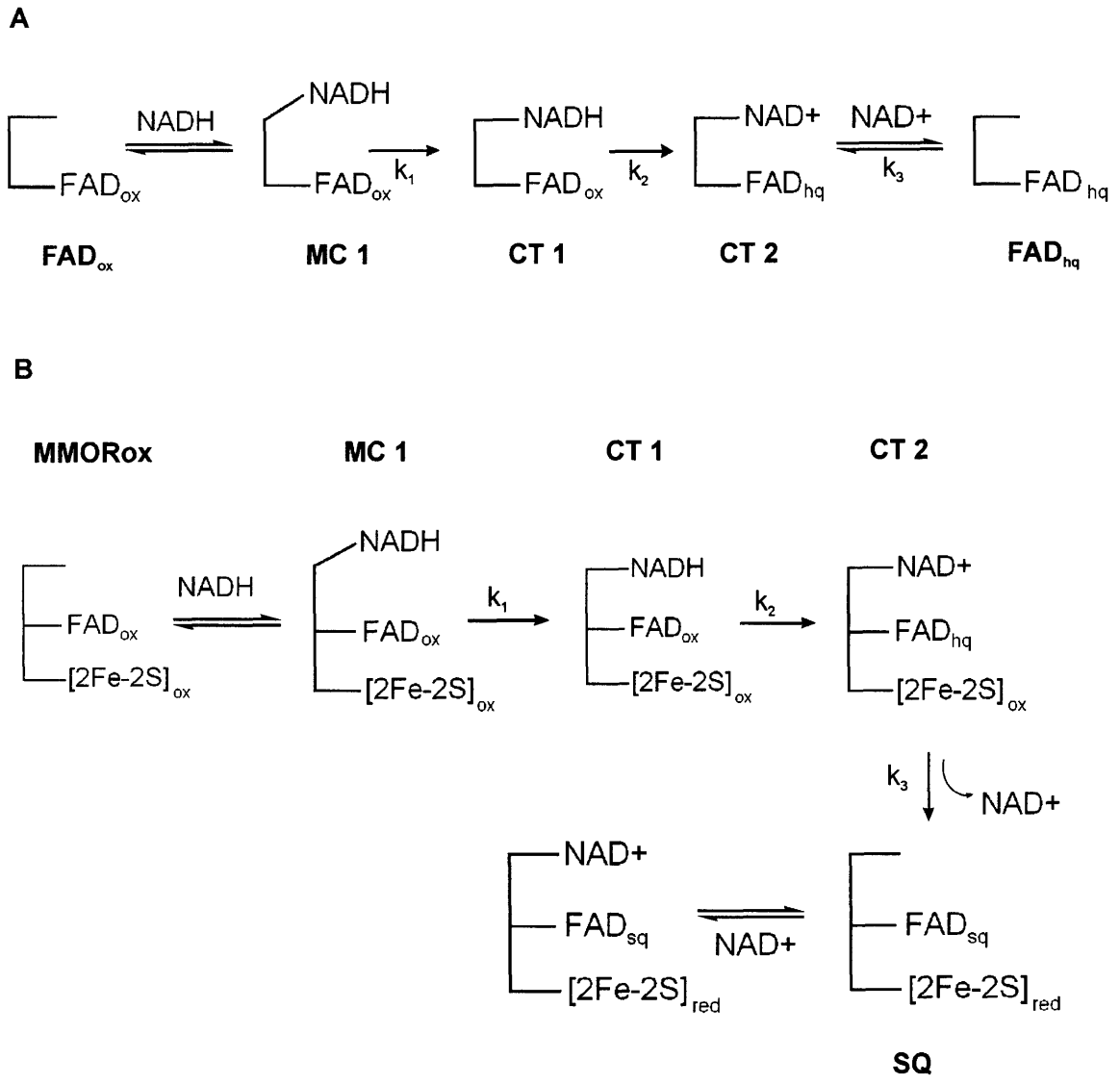

Scheme 2-1. NADH binding and electron transfer steps for (A) MMOR-FAD (22) and (B) full-length MMOR (23).

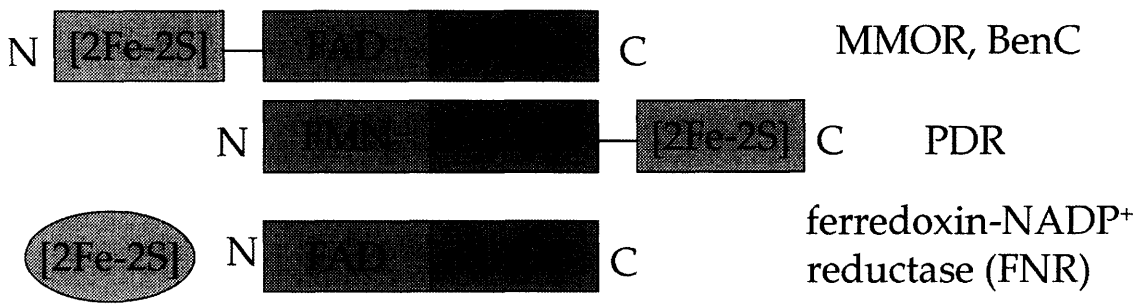

FIGURE 2-1. Domain arrangements of proteins in the ferredoxin-$NADP^+$ reductase subfamily. MMOR and BenC have a [2Fe-2S] ferredoxin domain linked at the N-terminus, while PDR has its ferredoxin domain linked as a C-terminal domain. Ferredoxin and FNR are expressed as separate proteins in photosynthetic organisms.

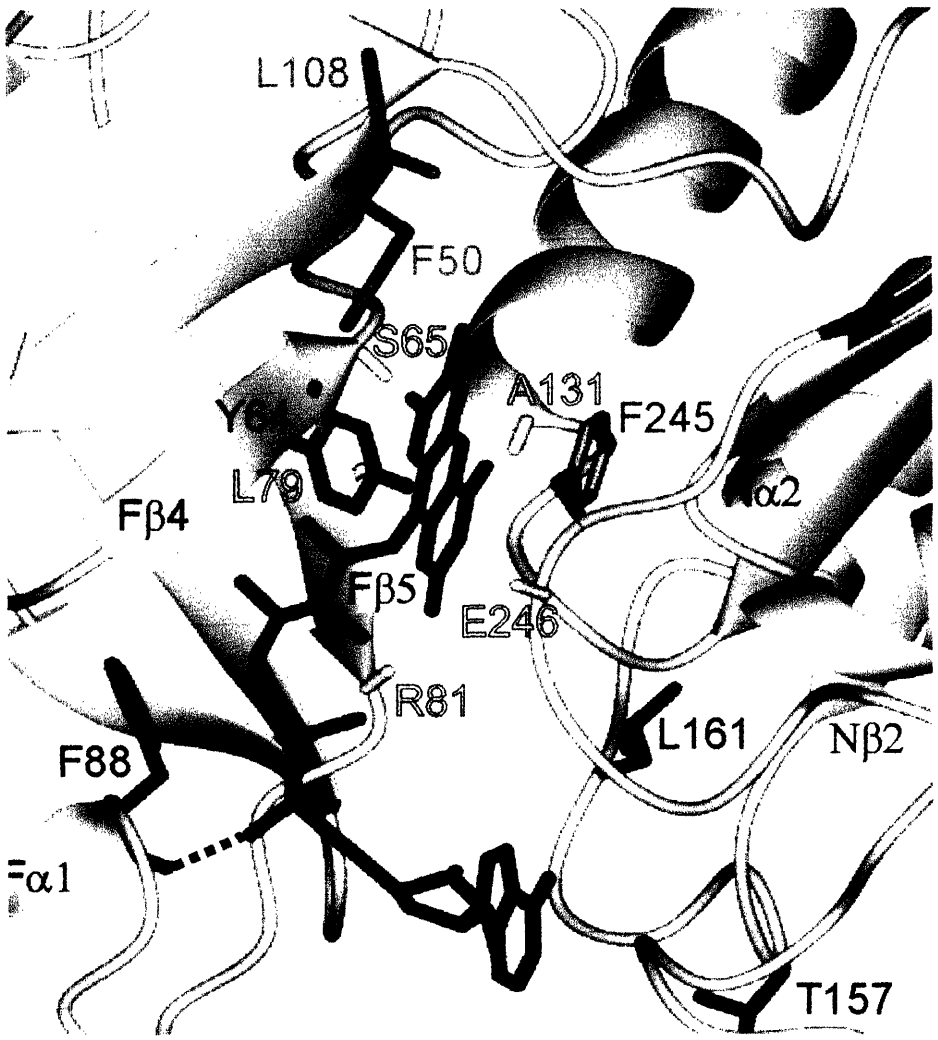

Figure 2-2. FAD Binding site of MMOR-FAD. Nearby residues with significant interactions are shown. Residue Phe 245, or Phe 342 in the full-length protein, is shown in orange, and is proposed to act as a conformational gate. In this structure of the reduced protein, the aromatic ring of Phe 245 is next to the flavin ring, blocking the nicotinamide binding site. This figure is taken from reference (16).

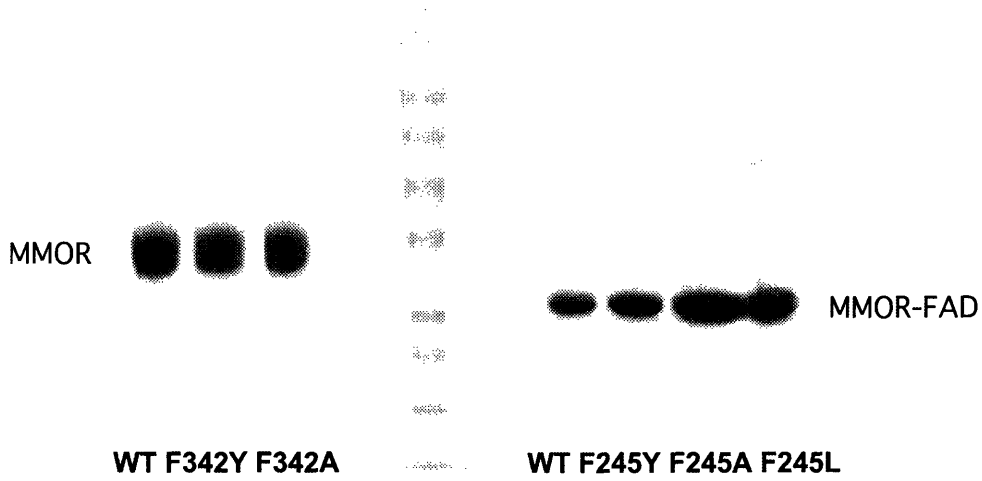

FIGURE 2-3. SDS-PAGE gel of purified MMOR and MMOR-FAD mutants. Proteins run as monomers on the gel, with molecular weights of 27 kDa for MMOR-FAD proteins and 37.5 kDa for MMOR proteins. The center lane contains molecular weight markers.

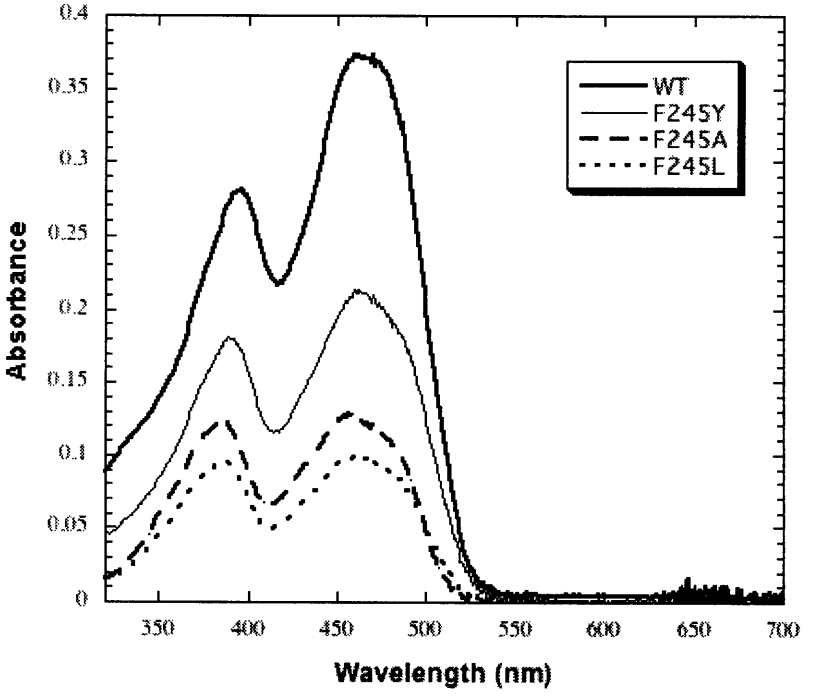

FIGURE 2-4. Spectra of MMOR-FAD wild-type protein and F245 mutants, characteristic of bound FAD. No significant shift is observed for the maximum at 458 nm, but there is a change in shifts of mutants for the peak at 396 nm in the wild-type protein.

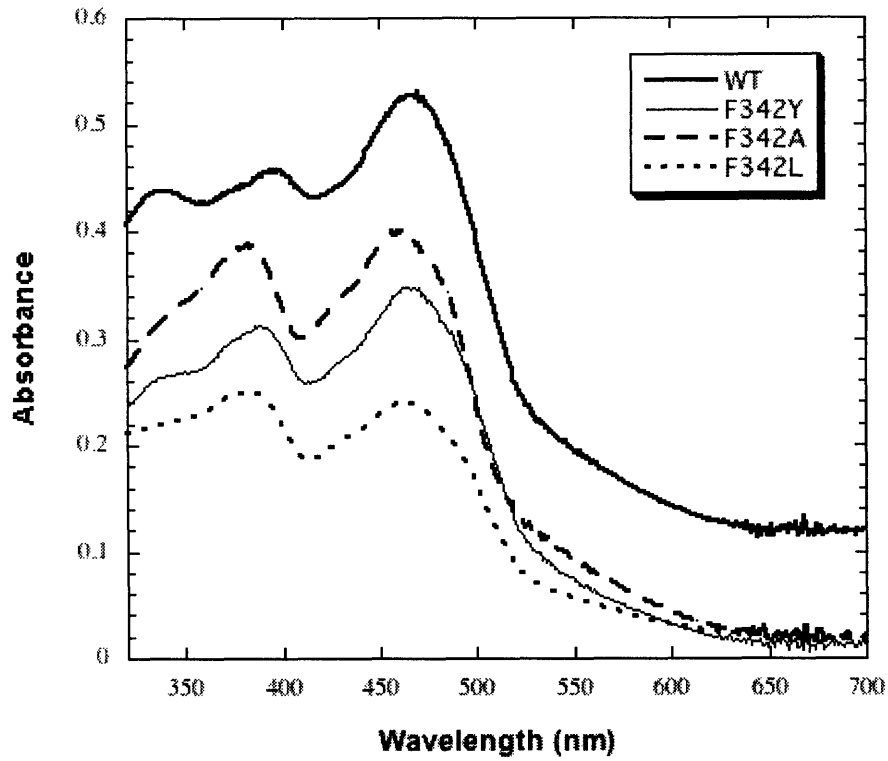

FIGURE 2-5. UV-Visible spectra of full-length MMOR wild-type protein and F342 mutants. There is a shift for the peak at 396 nm as observed for the F245 mutants. Additionally, the peak at 338 nm corresponding to the [2Fe-2S] cluster appears as a shoulder for F342Y and F342A, and is nonexistent for F342L.

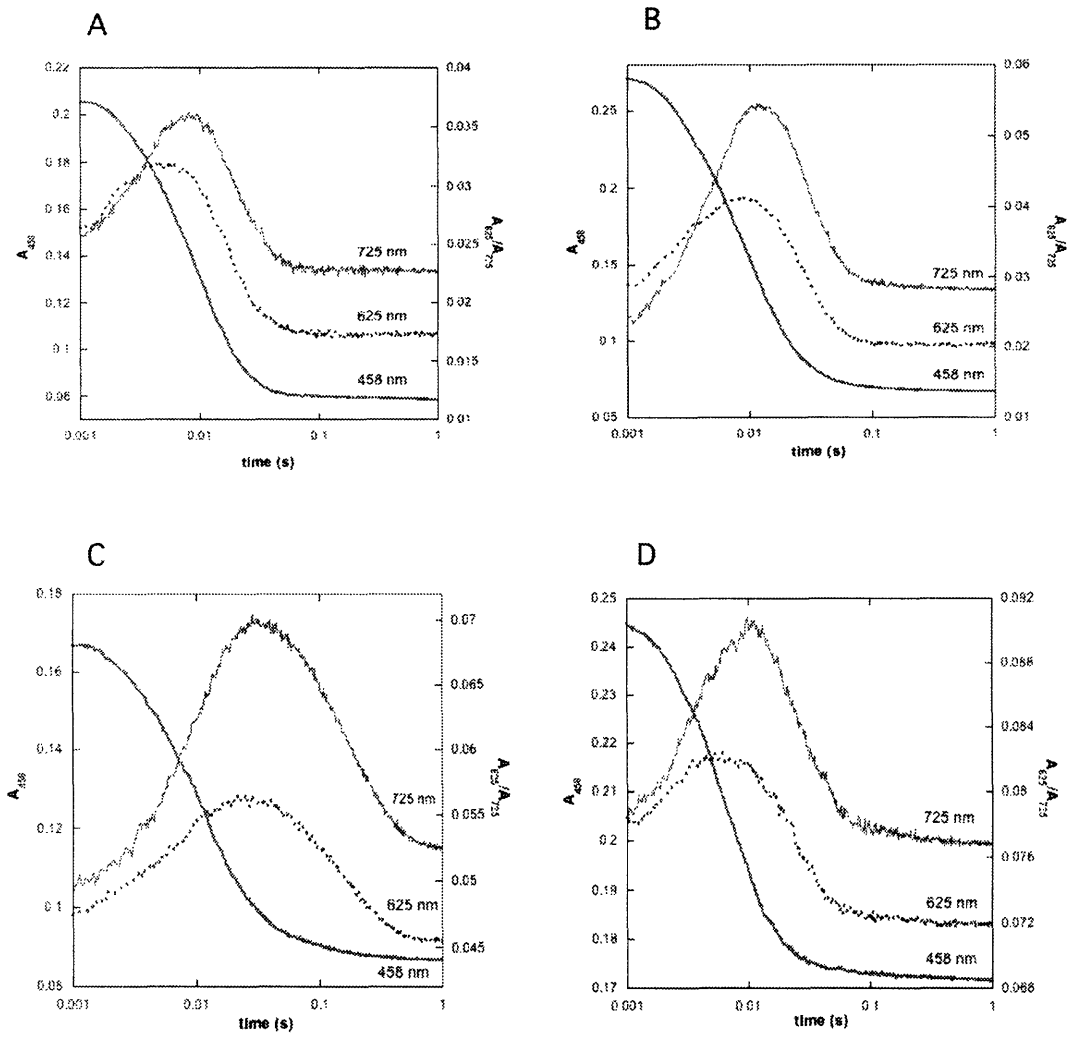

FIGURE 2-6. Single-wavelength stopped flow traces of (A)wild-type MMOR-FAD, (B) F245Y, (C) F245A and (D) F245L. Traces were followed at wavelengths of 458 nm, 625 nm and 725 nm as indicated above. All traces are shown on a logarithmic time scale.

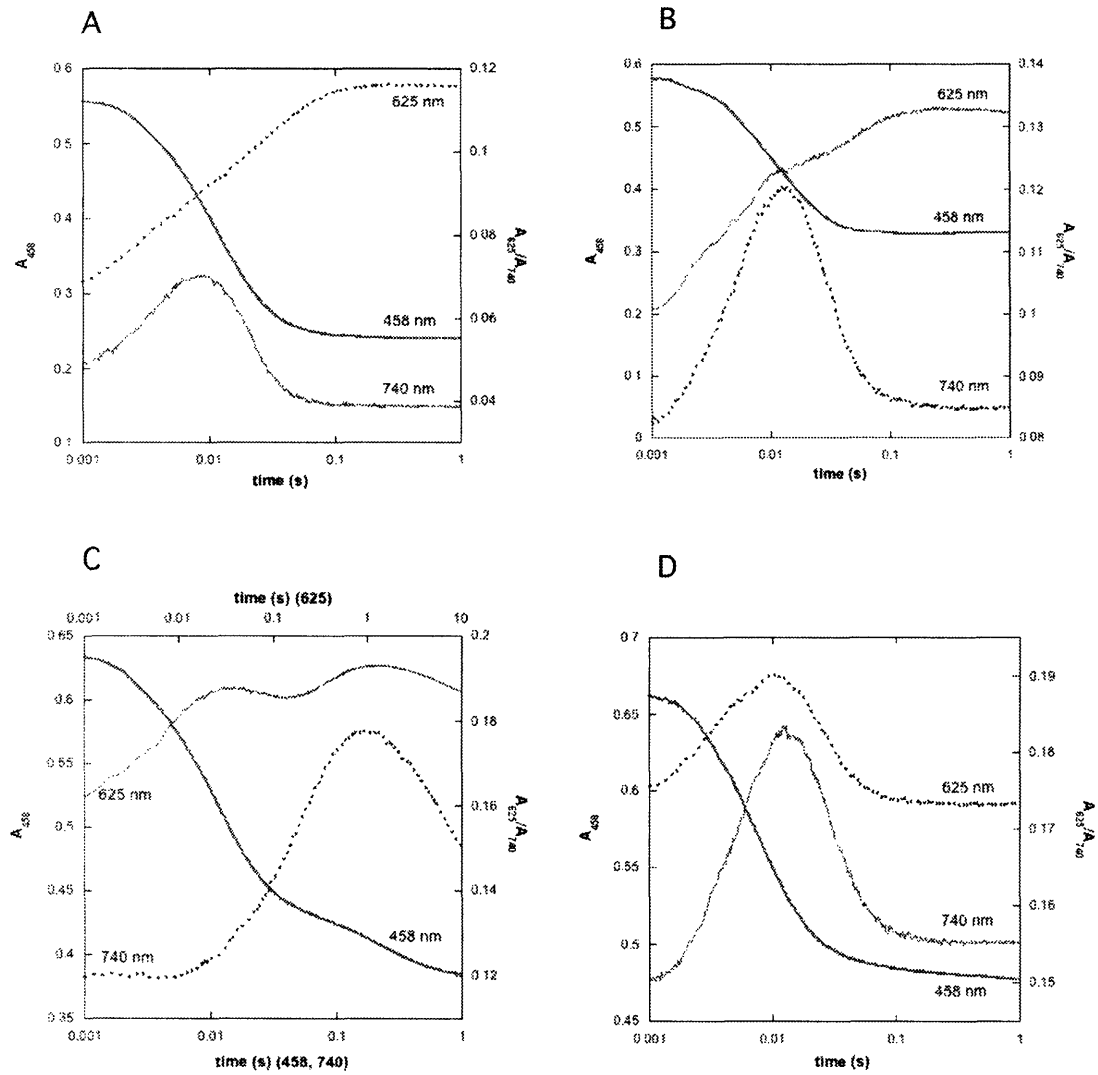

FIGURE 2-7. Single-wavelength stopped flow traces of (A)wild-type MMOR, (B) F342Y, (C) F342A and (D) F342L. Traces were followed at wavelengths of 458 nm, 625 nm and 740 nm as indicated above. All traces are shown on a logarithmic time scale.

BIOGRAPHICAL NOTE

The author was born on June 26, 1979 in Lima, Ohio, the daughter of Phillip and Sharon Chatwood. After graduating as valedictorian from Greenville High School in 1997, she attended Miami University in Oxford, Ohio as a Benjamin Harrison scholar. She earned several chemistry awards, including outstanding chemistry student, as well as being named a Goldwater scholar prior to graduating summa cum laude with a B.S. in biochemistry in 2001. A recipient of a National Science Foundation graduate fellowship, she attended the Massachusetts Institute of Technology to work in the laboratory of Professor Stephen Lippard. She is pursuing a pharmacy degree from the State University of New York at Buffalo.

Lisa L. Chatwood

Education

S.M., Biological Chemistry
GPA 4.80/5.00
2001-2004
Massachusetts Institute of Technology
Cambridge, MA

B.S., Biochemistry
Summa Cum Laude, GPA 3.90/4.00
1997-2001
Miami University
Oxford, OH

Awards

NSF Predoctoral Fellow
USA Today All-Academic Team Honorable Mention
Goldwater Scholar
Board of Trustees Harrison Scholar
Merck Award for Outstanding Senior Chemistry Student
Outstanding Inorganic Student
Outstanding Organic Student
Buckingham Scholarship (Chemistry)
Procter and Gamble Scholarship (Chemistry)
National Merit Scholar

Publications

Chatwood, L.L., Müller, J., Gross, J.D., Wagner, G., Lippard, S.J. (2004) NMR Structure of the Flavin Domain of Soluble Methane Monooxygenase from Methylococcus capsulatus (Bath) *Biochemistry,* in press.

Brandt, J.J., Chatwood, L.L., Crowder, M.W. (2000) Analysis of three overexpression systems for VanX, the zinc(II) dipeptidase required for high-level vancomycin resistance in bacteria. *Protein Expression and Purification* 20 (2), 300-307.

Yang KW, Brandt JJ, Chatwood LL, Crowder, M.W. (2000) Phosphonamidate and phosphothioate dipeptides as potential inhibitors of VanX. *Bioorganic and Medicinal Chemistry Letters* **10** (10), 1085-1087.

Brandt JJ, Chatwood LL, Yang KW, Crowder, M.W. (1999) Continuous assay for VanX, the D-Alanyl-D-Alanine dipeptidase required for high-level vancomycin resistance. *Analytical Biochemistry* **272** (1): 94-99.

Presentations

L.L. Chatwood, J. Müller, J.D. Gross, G. Wagner, S.J. Lippard. NMR structure of the FAD and NADH binding domains of the reductase component of soluble methane monooxygenase from Methylococcus capsulatus (Bath). 226th National ACS Meeting (New York, NY, September 2003).

L.L. Chatwood, J.J. Brandt, K.W. Yang, M.W. Crowder. VanX, a metalloenzyme conferring high-level vancomycin resistance. Ohio Inorganic Chemistry Graduate Student conference (Columbus, Ohio, November 2000).